

Doctoral Dissertation

A Systematic Histopathological Study of Duchenne Muscular Dystrophy Using Semi-Quantitative Image Analysis, Digital Restoration Techniques, and Exploratory Statistical Approaches

(デュシェンヌ型筋ジストロフィー筋生検標本の探索的統合解析による組織病理学研究)

, 2025

Hokkaido University

Tetsuhiro Yamakado

Doctoral Dissertation

A Systematic Histopathological Study of Duchenne Muscular Dystrophy Using Semi-Quantitative Image Analysis, Digital Restoration Techniques, and Exploratory Statistical Approaches

(デュシェンヌ型筋ジストロフィー筋生検標本の探索的統合解析による組織病理学研究)

, 2025

Hokkaido University

Tetsuhiro Yamakado

Index

List of Publications and Conference Presentations-----	1
Abstract-----	2
List of Abbreviations -----	6
Introduction -----	10
Materials and Methods -----	12
Results -----	23
Discussion-----	52
Conclusions -----	68
Acknowledgements -----	69
Conflicts of Interest-----	70
References-----	71

List of Publications and Conference Presentations

1. Publication

Part of this study has been presented in the following publication:

Yamakado T et al. "Myofiber Density Reveals a Critical Threshold around Age 6 in Steroid-Naïve Duchenne Muscular Dystrophy: A Retrospective Observational Study."

2. Conference Presentation

Part of this study has been presented at the following conference:

Tanei ZI, Yamakado T, Oda Y, Wang L, Tsuda M, and Tanaka S. Autopsy and research of the nervous system at Hokkaido University. The 114th Annual Meeting of the Japanese Society of Pathology, April 17, 2025, Sendai, Japan.

Abstract

Background and Objectives: Duchenne muscular dystrophy (DMD) is a severe X-linked neuromuscular disorder marked by progressive muscle degeneration and significant cardiopulmonary complications. Despite therapeutic advances significantly improving patient outcomes, critical gaps remain in understanding early-stage DMD pathophysiology. Systematic investigations into early-stage histopathological changes remain limited. A previous study has proposed a critical histological period around ages 6–7, marked by rapid increases in connective tissue, implying relative histological stability before this interval. Initially skeptical, this hypothesis was questioned due to the absence of corresponding physiological phenomena around this specific age interval and the significantly earlier onset of clinical symptoms (typically between ages 3 and 5 years). Recognizing this significant clinicopathological discrepancy, this study aimed to resolve this contradiction. This study leveraged severely deteriorated archival muscle biopsy specimens obtained more than 40 years ago, without accompanying clinical records, from the former Yakumo National Hospital (now integrated into Hokkaido Medical Center, Japan). This study aimed to establish novel histopathological markers, clarify early disease mechanisms, and elucidate meaningful clinicopathological correlations in early-stage DMD based solely on histopathological findings and age at biopsy (ABx).

Materials and Methods: This retrospective observational study adhered to the Declaration of Helsinki and was approved by the institutional review board of Hokkaido University Hospital (No. 024-0310), which oversees Hokkaido Medical Center. The requirement for informed consent was waived due to the retrospective study design. Archival muscle biopsy slides (quadriceps femoris muscle) of steroid-naïve DMD patients diagnosed between 1973 and 1984 were reviewed. Due to limitations in clinical record availability, initial selection partially relied on historical recollections. A total of 46 biopsy were evaluated among three pathologists. Histological slides (frozen and formalin-fixed paraffin-embedded) stained with hematoxylin-eosin (H&E), Gomori trichrome (G-T), and Masson trichrome (M-T) underwent digital restoration using look-up tables (LUTs) and Focus Stacking techniques. Actomyosin adenosine triphosphatase (ATPase)-stained slides were not included in primary analysis but used in sensitivity analyses. Quantitative morphometric analyses, such as myofiber size (MFS)-related metrics (e.g., standard deviation of MFS (Sd), coefficient of variation of MFS (Cov)),

myofiber density (*MFD*), myofiber area (*MFA*), connective/fibrotic tissue area (*CFA*), were performed using Adobe Photoshop. Statistical analyses involved preliminary comparisons of staining methods, correlation analyses, and multiple regression modeling to predict *ABx*. Model fit was assessed by calculating Akaike's information criterion (AIC), and prediction accuracy was validated by calculating the root mean squared error (RMSE) through leave-one-out cross-validation (LOOCV). Model residuals were analyzed to identify prediction error patterns across predefined age intervals (1–4, 1–6, 6–7, 7–9, 9–11, and 11–17 years) using the Kruskal-Wallis test. Group differences were tested using analysis of variance (ANOVA) or non-parametric methods depending on data distribution, along with effect size analysis. Logistic regression was performed to identify critical thresholds of the parameters of interest at age 6. Segmented regression was performed to determine the existence of an age-related inflection point in dynamics of each parameter. Bayesian statistical analyses and Monte Carlo simulations were subsequently conducted to confirm the robustness and estimate the sample size. A significant threshold of $p < 0.05$ was applied to all statistical tests.

Results: A preliminary paired analysis revealed no significant difference in *MFA* between H&E and G-T staining (Cliff's δ : 0.015 [confidence interval (CI) −0.28, 0.31]; negligible), with strong correlation confirming interchangeability (Pearson's $r = 0.970$, $p < 0.001$); comparison with M-T staining was precluded by limited sample size. Bayesian analysis also confirmed negligible batch effects. Subsequently, from 46 muscle biopsies, 38 samples (patients aged 1–16 years) met the inclusion criteria. Histopathological evaluation demonstrated marked reductions in *MFD* with increasing age, alongside characteristic DMD features including increased connective tissue, variability in MFS, fatty infiltration, and internally nucleated and/or hypercontracted fibers. Correlation analyses identified *MFD* as the strongest predictor inversely correlated with *ABx* ($\rho = -0.85$). Multiple regression established robust age-prediction models, predominantly driven by *MFD* and its interaction with *Sd* (adjusted $R^2 = 0.79$). This full-range model (all ages included) yielded an AIC of 53.84 and an RMSE of 0.49. The results of Kruskal–Wallis tests demonstrated that model accuracy significantly declined in older age groups ($p < 0.01$). Consequently, an alternative model limited to patients younger than 7 years was evaluated, revealing a markedly improved fit (AIC = 29.12) and comparable RMSE (0.47). When stratified by age groups (1–6 years, $n = 13$; 6–7, $n = 8$; 7–11, $n = 14$) in ANOVA, *MFD* exhibited substantial differences between groups (Glass's $\Delta = -1.75$ [CI −2.85, −1.25] for ages 1–6 vs. 6–7; -1.81 [CI −2.91, −1.35] for

1–6 vs. 7–11). Other key parameters, such as MFS-related parameters, *MFA*, and *CFA*, also exhibited significant differences between age groups 1–6 and ≥ 7 years. Replacing *MFD* values with measurements from ATPase-stained slides further supported these findings. Logistic regression revealed statistically significant *MFD* thresholds of 546–572 fibers/mm² differentiating patients below or above age 6. Segmented regression identified a breakpoint at age 6.25 [CI 5.08, 7.42], with Bayesian analysis and Monte Carlo simulations further confirming statistical support for this threshold and sufficient statistical power (approximately 80% probability of detecting the breakpoint within \pm 1.25 year). Supplemental piece-wise variance analysis stratified by breakpoint CI confirmed cross-parameter validity.

Discussion: These findings challenge previous views by demonstrating rapid *MFD* decline significantly before age 6, indicating a previously unrecognized subclinical phase of accelerated myofiber loss. Methodologically, employing archival biopsy specimens, innovative image restoration techniques were applied to recover faded histological details. These techniques confirmed *MFD* as a robust marker with clear histopathological significance. Exploratory statistical analyses incorporating regression modeling and prediction error analyses revealed precise age-related histopathological shifts. An alternative regression model restricted to patients younger than approximately 7 years predicted *ABx* more accurately, highlighting increased variability in disease progression beyond this age. Variance analysis demonstrated superior sensitivity of *MFD* compared to conventional histological indices. Exploratory logistic regression identified *MFD* thresholds distinguishing patients younger and older than age 6. Segmented regression confirmed the breakpoint around age 6. These thresholds closely align with clinically observed functional declines around ages 6–7 years, reinforcing a critical therapeutic window. Thus, *MFD* could inform optimal timing for initiating corticosteroids and novel therapies. Development of noninvasive monitoring tools, such as radiomics and deep learning image analysis, is anticipated in clinical management. Importantly, whether the reduced *MFD* after age 6 signifies irreversible muscle pathology or if therapeutic interventions can effectively reverse these changes, underscoring the need for continued investigation. Collectively, this study underscores the importance and inherent challenges of developing novel evaluation frameworks outside established analytical paradigms, delineating novel histopathological hallmarks of early-stage DMD and informing future therapeutic strategies.

Conclusions: This study established *MFD* as a sensitive biomarker for early-stage DMD, identifying a previously unrecognized phase of rapid myofiber loss before age 6. This threshold age may represent a critical histopathological turning point in disease progression. Future research should prioritize longitudinal, multicenter studies to validate the robustness of *MFD* dynamics. The author believes that the present findings promote the broader utilization of archival specimens in future translational research, thereby refining the understanding of the DMD's pathophysiology and enhancing clinical decision-making for this devastating neuromuscular disorder.

List of Abbreviations

***ABx* (parameter)**

age at biopsy

AIC

Akaike's Information Criterion

ANOVA

analysis of variance

ATPase

actomyosin adenosine triphosphatase

BF₁₀

Bayes Factor (alternative hypothesis "1" over null hypothesis "0")

BIC

Bayesian Information Criterion

***CFA* (parameter)**

connective/fibrotic tissue area

ClIs

confidence intervals

CK

creatine kinase

***Cov* (parameter)**

the coefficient of variation of myofiber size

CrI

credible interval

DMD

Duchenne muscular dystrophy

***Fat* (parameter)**

fatty degeneration area

FFPE

formalin-fixed paraffin-embedded

FOIs

fields of interest

G-T

Gomori-Trichrome

H&E

Hematoxylin-Eosin

***IntN* (parameter)**

percentage of internally nucleated fibers relative to *MFD*

LED

light-emitting diode

LOESS

Locally Estimated Scatterplot Smoothing

LOOCV

leave-one-out cross validation

looIC

leave-one-out information criterion

LUTs

Look-Up Tables

***Mean* (parameter)**

mean MFS

***MFA* (parameter)**

myofiber area

***MFD* (parameter)**

myofiber density

MFS

myofiber size

M-T

Masson-Trichrome

***NFA* (parameter)**

necrotic fiber area

***Opaque* (parameter)**

percentage of opaque fibers relative to *MFD*

ORs

odds ratios

PCR

polymerase-chain reaction

***RFA* (parameter)**

regenerative fiber area

RMSE

root mean squared error

ROPE

Region of Practical Equivalence

SD

standard deviation

***Sd* (parameter)**

standard deviation of MFS

Introduction

Background

The inception of this research originated from the concept that historical muscle biopsy slides, especially those from patients with Duchenne muscular dystrophy (DMD) preserved at the former National Yakumo Hospital (currently integrated into the National Hospital Organization, Hokkaido Medical Center, Sapporo, Hokkaido, Japan), could be valuable for further investigative purposes. As well described until today, DMD is a severe X-linked neuromuscular disorder characterized by progressive skeletal muscle degeneration, ultimately leading to profound muscle weakness and cardiopulmonary complications (Birnkrant et al., 2018a, 2018b, 2018c; Crisafulli et al., 2020; Duan et al., 2021).

Historically, respiratory failure was the leading cause of death in DMD patients; however, with advances in assisted ventilation, cardiac failure has become predominant (Birnkrant et al., 2018b; Nonaka and Nishino, 2021). Despite significant advancements in therapeutic interventions and disease management (Bez Batti Angulski et al., 2023; Biggar et al., 2022; Birnkrant et al., 2018a, 2018b, 2018c; Duan, 2018; Duan et al., 2021; Elangovan and Dickson, 2021; Erkut and Yokota, 2022; Frank et al., 2020; Happi Mbakam et al., 2022; Matthews et al., 2016; Mendell et al., 2020, 2013; Min et al., 2019; Sun et al., 2020; Takeda et al., 2021; van Dommelen et al., 2024), notable gaps remain in the current understanding of early-stage DMD pathophysiology, particularly regarding the establishment of reliable histopathological markers for disease progression.

What is Known and Unknown

Briefly, although histological evaluation is recognized as essential for understanding DMD pathology within the field of muscle histopathology (Bell and Conen, 1967; Desguerre et al., 2009; Dubuisson et al., 2022; Peverelli et al., 2015), surprisingly little is known about the detailed histopathological changes occurring during the early stages of DMD. At the beginning of this study project, conducting a thorough review of previously established histopathological findings was therefore critical. However, systematic investigations into histopathological correlations in DMD remain limited, with most studies primarily assessing myofiber cross-sectional area and fibrotic changes (Cardone et al., 2023; Desguerre et al., 2009; Peverelli et al., 2015).

The study by Peverelli et al. exerted significant influence on initial research

design, prompting to initially adopt methodologies similar to their image analysis approach (Peverelli et al., 2015). Central to their findings was the hypothesis of a critical period at ages 6–7 years characterized by a rapid increase of connective tissue, suggesting that histological muscle architecture remains largely unchanged until approximately this age.

This critical period hypothesis was profoundly skeptical for this study from the outset; the skepticism stemmed primarily from the lack of any known significant physiological events around 6–7 years of age. Had there been any established physiological phenomena—such as a marked increase in muscle strength or growth spurt—coinciding precisely with this age range, such a claim might have been more convincing. However, no such physiological basis has been reported. Additionally, clinical manifestations of DMD clearly emerge much earlier than this proposed critical period. For instance, early clinical manifestations—including stair-climbing difficulties, waddling gait, and frequent falls—typically emerge between 3 and 5 years of age (Birnkrant et al., 2018b; Crisafulli et al., 2020; van Dommelen et al., 2024), with contractures of the iliotibial bands, hip flexors, and heel cords becoming apparent before the age of 6 years (Brooke et al., 1983). It was concluded that existing histopathological findings at this time could not adequately explain the pathophysiology of DMD.

Purposes

Given this context, resolving the profound discrepancy—a severe "clinicopathological dissociation"—became a crucial challenge for this study. The only resources available for this study were significantly deteriorated archival specimens prepared over 40 years ago, lacking any accompanying clinical information (e.g., assessments of motor and/or physical function, serum creatine kinase (CK) levels). Nevertheless, under these constraints, relying solely on histopathological findings and biopsy age, this study aimed to establish novel histopathological markers, clarify early disease mechanisms, and elucidate clinically meaningful correlations in early-stage DMD, ultimately informing diagnostic precision and clinical decision-making.

Materials and Methods

Standard Protocol Approvals, Registrations, and Patient Consents

All procedures performed in this retrospective observational study involving human participants were conducted in accordance with the ethical standards of the institutional and national research committee, as well as the 1964 Declaration of Helsinki and its later amendments, and complied with the Ethical Guidelines for Medical and Biological Research Involving Human Subjects established by the Ministry of Education, Culture, Sports, Science and Technology and the Ministry of Health, Labor and Welfare, Japan. The study was approved by the central institutional review board of Hokkaido University Hospital (Approval No. 024-0310, Sapporo, Hokkaido, Japan), which also oversees the National Hospital Organization Hokkaido Medical Center as part of its centralized review process. Due to the retrospective nature of the study, the requirement for informed consent was waived by the ethics committee.

Samples

Initially, archival muscle biopsy slides had been stored under suboptimal conditions at an off-site storage facility, and clinical records were largely unavailable or incomplete. Therefore, preliminary selection of biopsy samples was partly informed by recollections provided by former nurses familiar with patient histories at the Yakumo National Hospital. Subsequently, clinical records retrieved from the hospital archives were reviewed to confirm basic patient information, ultimately enabling the identification and screening of a total of 46 muscle biopsy slides obtained from the quadriceps femoris muscles of patients diagnosed with DMD between 1973 and 1984.

Due to inherent limitations imposed by the retrospective nature of this study and the condition of available archival specimens, the inclusion criteria were inevitably determined as follows: (1) pathological and clinical confirmation of DMD, with genetic verification when feasible after the introduction of genetic testing around the year 2000; (2) patient treatment history at the former Yakumo National Hospital (subsequently integrated into Hokkaido Medical Center in 2020, as described) from 1968 to the present; (3) absence of prior corticosteroid treatment at the time of biopsy; and (4) sufficient tissue quantity and acceptable slide quality, confirmed through evaluation involving the author and two other independent pathologists. Slides failing to meet these criteria were excluded from analysis. Patients with Becker muscular dystrophy were not included in the study. Archival specimens consisted of frozen-section slides, formalin-

fixed paraffin-embedded (FFPE) blocks, or both, depending on case availability. Histological staining techniques applied to the specimens included hematoxylin-eosin (H&E), Gomori trichrome (G-T), and Masson trichrome (M-T); however, not all slides were available with each staining method. Actomyosin adenosine triphosphatase (ATPase)-stained slides were not used for the primary analysis, but served to support the statistical validation and sensitivity analyses.

Study Devices and Settings

As described later, since this study utilized a look-up table (LUT)-based digital restoration method, it was anticipated that reproducibility would be significantly affected by variations in color temperature. Thus, it was essential to use a microscope equipped with a light-emitting diode (LED) illumination system to ensure consistent results. Therefore, microphotographic imaging was performed using a Nikon ECLIPSE Ci microscope, which utilizes LED illumination system, equipped with a Nikon PLAN APO λD 40 \times objective lens and a Nikon DS-Fi3 camera, in conjunction with Nikon NIS-D software (Nikon Corporation, Inc., Tokyo, Japan).

Fields of interest (FOIs) for image analysis were jointly selected by the three pathologists. High-resolution images were acquired at 400 \times magnification (2,880 \times 2,048 pixels; resolution: 0.11 $\mu\text{m}/\text{pixel}$) and subsequently compiled into large composite images consisting of 16 tiled frames (final image resolution: 11,520 \times 8,192 pixels), corresponding to a 1.14 mm² field of view under a 10 \times objective lens. Semi-quantitative digital image analysis was performed using Adobe Photoshop 2024 (Adobe Systems, Inc., San Jose, CA, USA), a software widely used in histopathological research (Ding et al., 2022; Egan et al., 2012; Fitzgerald et al., 2019; Zhou et al., 2017).

Morphometric Analyses and Quantifications

Although the differentiation between normal and abnormal myofibers (e.g., normal/total myofiber area measurement and normal/total myofiber counting) was initially attempted, thereby adopting a semi-quantitative analytical approach, subsequent evaluations raised concerns regarding the reproducibility, necessity, and validity of distinguishing myofiber states based on qualitative criteria. Consequently, the parameter definitions were revised and finalized as described below, emphasizing fully quantitative and reproducible measures.

In this study, each parameter used in the statistical analysis is highlighted by capitalizing the initial letter and italicizing it for clarity (e.g., *Parameter*). Initially, four

indices primarily assessing myofiber size (MFS) were introduced:

- (1) The mean MFS (*Mean*, μm^2);
- (2) The standard deviation of MFS (*Sd*, μm^2);
- (3) The coefficient of variation of MFS (*Cov*); and
- (4) Myofiber density (*MFD*, fibers/ mm^2), which was derived as an auxiliary metric during the enumeration of individual fibers while evaluating MFS-related parameters, regardless of pathological features (e.g., central nucleation, hypercontraction).

Additionally, seven conventional morphometric parameters, established in previous studies (Desguerre et al., 2009; Dubuisson et al., 2022; Peverelli et al., 2015), were analyzed, each expressed as a percentage per FOI unless otherwise specified:

- (1) Myofiber area (*MFA*), similarly regardless of pathological features;
- (2) Connective/fibrotic tissue area (*CFA*);
- (3) Necrotic fiber area (*NFA*);
- (4) Regenerative fiber area (*RFA*);
- (5) Fatty degeneration area (*Fat*);
- (6) Percentage of opaque fibers relative to *MFD* (*Opaque*, count/*MFD*, %); and
- (7) Percentage of internally nucleated fibers relative to *MFD* (*IntN*, count/*MFD*, %).

To enhance image quality and facilitate accurate morphometric analysis, color restoration was performed using LUTs in Nikon NIS-D software, a tool commonly employed in fluorescence and confocal microscopy (Li et al., 2011; Sanderson et al., 2014). High-resolution images at $400\times$ magnification were acquired in real-time using LUTs and subsequently tiled to generate a composite large-image (**Figure 1A**). LUTs not only facilitated the identification of *IntN* and *Opaque* but also clearly delineated myofiber boundaries, fatty infiltration, and other histological changes (**Figure 1B**).

To mitigate artifacts arising from focal plane variations, Focus Stacking (Jütte et al., 2022) using a script in Adobe Photoshop was implemented. The application of Focus Stacking to histopathological microscopy was inspired by a photographic technique developed for capturing uniformly focused images of objects such as pumpkin skin from multiple focal planes (Shosekai-Kenkyujo, 2021). This technique combined multiple images captured at varying focal depths into an extended depth-of-field composite image (**Figure 1C**).

Artifact regions that could not be rectified using these methods were excluded

from the FOI. Myofiber tracing utilized Magnetic Lasso Tool in Adobe Photoshop (contrast: 40, frequency: 100), and MFS-related parameters were measured using a monochrome-converted image to enhance contrast and accuracy (**Figure 1D**).

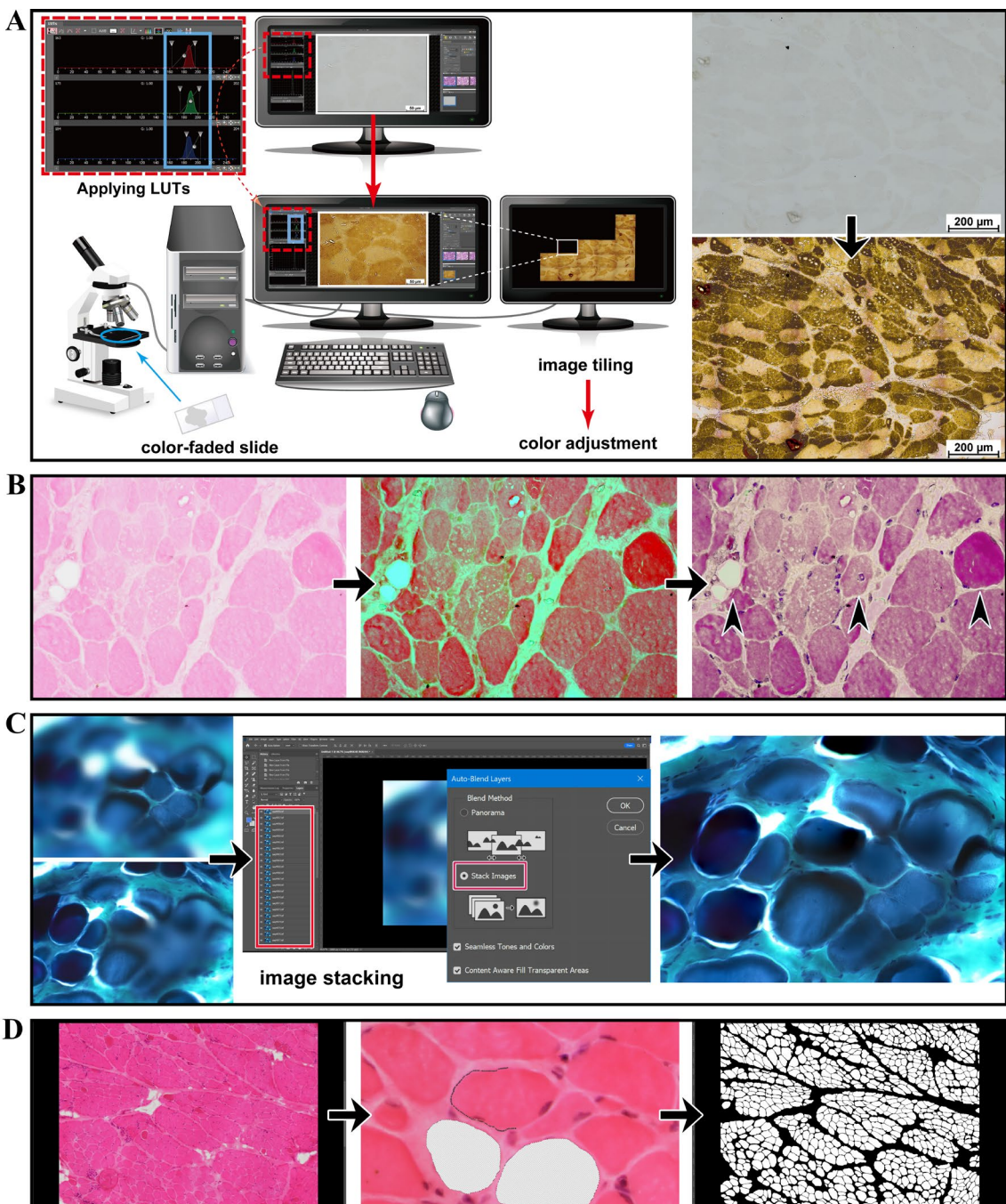


Figure 1: Sequential workflow for progressive restoration and semi-quantitative image analysis

A: This panel illustrates the application of LUTs to digitally restore a severely faded ATPase-stained specimen (pH 9.4), representing the most extensively degraded example

in this study's series. Adjusting LUTs in the live camera preview mode enhances the visibility of tissue structures that have faded over time. The processed images are subsequently tiled to generate a high-resolution, composite image encompassing the entire FOI. Next, commonly used color adjustment functions in Photoshop (e.g., Color Balance, Hue/Saturation) effectively restore an ATPase-like appearance. This restoration technique, originally developed for ATPase-stained slides, provided a foundation for refining the methodology for additional histological stains, as demonstrated in subsequent panels.

B: The restoration approach described in panel **A** is adapted for H&E staining, in which nuclear structures are difficult to discern as a result of fading. Initially, LUTs are applied, rendering otherwise undetectable nuclei in green, thereby improving the visualization of nuclear morphology and myofiber boundaries. Subsequently, color adjustment functions in Photoshop are employed to transform the green-highlighted nuclei into a purple hue, thereby restoring an appearance characteristic of H&E staining. This approach facilitates the clear identification of features such as centrally nucleated and hypercontracted myofibers, as well as areas of fatty infiltration, become clearly discernible (arrowheads). Both panels (**A** and **B**) illustrate the same core process—using LUT-based digital enhancement and subsequent color adjustments—to recover faded tissue details.

C: Focus Stacking is employed to enhance the visualization of a G-T-stained specimen. Multiple images are captured at varying focal depths and subsequently combined into a single, sharply focused image using the Auto-Blend Layers function in Adobe Photoshop. This process generates a uniform, high-resolution image that effectively preserves the intricate structural details of the myofibers.

D: This panel demonstrates the use of the Magnetic Lasso Tool in Adobe Photoshop to delineate individual myofibers in an H&E-stained specimen. A subtle LUT-based adjustment was applied beforehand to slightly enhance image contrast, facilitating accurate tracing of myofiber boundaries. The segmented image is subsequently converted into a monochrome format to simplify visualization and facilitate quantitative analysis. MFS (px^2 , initially) is measured, and the MFS along with the standard deviation are calculated using Microsoft Excel (Microsoft Corporation, Redmond, WA, USA).

*Note: The illustration in panel **A** was generated using Adobe Illustrator software (Adobe Systems, Inc., San Jose, CA, USA) and incorporates freely available resources from Pixabay (<https://pixabay.com>) alongside screenshots of the Nikon NIS-D software*

interface (Nikon Corporation, Inc., Tokyo, Japan). This figure also includes screenshots of Adobe Photoshop (Adobe Systems, Inc., San Jose, CA, USA), which was used in the image analysis workflow (panels **C** and **D**).

(**Abbreviations:** LUTs, look-up table; ATPase, actomyosin adenosine triphosphatase; FOI, field of interest; H&E, hematoxylin-eosin; G-T, Gomori trichrome; *MFA*, myofiber area; MFS, myofiber size.)

Individual myofiber areas were quantified using the Analysis function in Adobe Photoshop, in which each myofiber was independently delineated to prevent measurement errors arising from overlapping or contiguous fibers. The function assigned unique labels to each selected region of interest, which were subsequently used to compute all parameters following the methodology previously described. Morphometric data extracted from Adobe Photoshop were exported as text files, further processed in Microsoft Excel, and saved in CSV format for statistical analysis.

Statistical Analyses

All statistical analyses were performed using R software (version 4.3.2). The analytical procedures are summarized as follows:

Preliminary Estimation between Different Staining Methods

Two frozen staining methods were compared: H&E and G-T staining. As described, due to limitations in sample availability, this study included H&E-, G-T-, and M-T-stained slides. To verify the comparability between these staining methods, *MFA* values were initially evaluated obtained from both methods using paired analyses. First, a small preliminary sample set ($n = 16$) was compared using Wilcoxon signed-rank tests and power analysis to estimate the required sample size for adequate statistical power. Subsequently, the evaluation was expanded to a larger paired-sample set and the Wilcoxon signed-rank test was performed.

Additionally, Pearson's product-moment correlation coefficients were calculated to further validate methodological interchangeability between the two staining methods. Due to limited slide availability, comparative analyses involving M-T staining, as well as comparisons between frozen and FFPE sections, could not be performed. Furthermore, practical equivalence between H&E and G-T staining was quantified by a Bayesian paired-sample t-test (Jeffreys–Zellner–Siow Cauchy prior with scale parameter $r = 0.707$) (Rouder et al., 2009). A Region of Practical

Equivalence (ROPE) of $|d| < 0.30$ was applied (Lakens, 2022); practical equivalence was concluded when $\geq 80\%$ of the posterior mass fell inside the ROPE and Bayes Factor ($BF_{10} < 1$). Additionally, a linear mixed-effects model with the paired observations clustered by specimen subject number was fitted, and changes in the specimen-level variance component (τ^2) were examined when staining method was added as a fixed effect.

Correlation Analyses

Bivariate correlation analyses using Spearman's rank correlation coefficients were performed to assess relationships between each quantified parameter and age at biopsy (ABx).

Multiple Regression Analysis

All variables were treated as continuous and transformed them into logarithmic scales followed by centering and/or z-score standardization. Multiple regression analysis with stepwise selection was performed to identify significant predictors for similarly transformed ABx . Potential interaction terms between variables were also explored. Akaike's information criterion (AIC) and model diagnostics, including residual plots, QQ plots, and Cook's distance, were examined to ensure the assumptions and reliability of the regression models. Additionally, to quantitatively evaluate the robustness and predictive reliability of the established regression models, the root mean squared error (RMSE) was calculated with a standard deviation (SD) and leave-one-out cross-validation (LOOCV) was conducted.

Residual (Predictive Error) Analysis

An original residual analysis approach was developed and applied based on prediction errors (residuals) derived from the multiple regression model. Specifically, the distribution of prediction errors were compared across the following predefined age intervals: 1–4, 4–6 (or 1–6), 6–7, 7–9, 9–11 (or 7–11), and 11–17 years, using the Kruskal–Wallis test. The rationale for these detailed age groupings was based on three primary considerations: (1) clinical symptoms typically manifest before age 6 years (Birnkrant et al., 2018b); (2) previous studies have hypothesized that a critical disease progression phase occurs around ages 6–7 years (Peverelli et al., 2015); and (3) to achieve a relatively balanced distribution

of sample sizes within each age group, with the exception of the oldest group (11–17 years). Furthermore, to verify the stability and predictive accuracy of the regression model within the younger age groups (up to 7 years), additional validation was performed using RMSE values obtained through LOOCV.

Initial Age Grouping

Based on the results described above, participants were subsequently stratified into the following age groups: 1–6 years, 6–7 years, and 7–11 years. Age group of 11–17 years was excluded due to the small sample size (see Results section).

Tests for Normality and Variance

The Shapiro–Wilk test was employed to evaluate data normality, while Levene's test assessed the homogeneity of variances for each variable.

Comparisons among Age Groups (1–6, 6–7, and 7–11 years)

For normally distributed data with homogeneous variances, analysis of variance (ANOVA) was performed, followed by Tukey's HSD post-hoc test. For non-normally distributed data, the Kruskal–Wallis test was applied, with post-hoc comparisons performed using the Conover test, incorporating Bonferroni correction. In cases where normality was assumed but variance homogeneity was not met, Welch's ANOVA was used, followed by the Games–Howell post-hoc test.

Effect Sizes

Effect sizes between groups were calculated based on data distribution characteristics. For variables satisfying assumptions of normality and homogeneity of variance, Hedges' d with bootstrapped confidence interval (CI) (5,000 iterations) was calculated based on the approach described by Nakagawa and Cuthill (Nakagawa and Cuthill, 2007). For variables meeting normality but violating the homogeneity of variance assumption, Glass's Δ with bootstrapped CIs was calculated. For variables that violated the assumption of normality, Cliff's δ with bootstrapped CIs was employed. Additional analyses were conducted by excluding extreme outliers to assess the robustness of statistical findings, where appropriate. Additionally, post-hoc power analysis was conducted to confirm whether the sample sizes provided sufficient statistical power (target statistical power: 80%).

Logistic Regression Analysis

For patients <11 years, logistic regression was employed to evaluate the relationship between the values of the parameter of interest and ABx , using 6 years as the reference point. Model fit was assessed using AIC, and predictive accuracy was assessed through odds ratios (ORs) with corresponding 95% CIs. To address multiple comparisons, Bonferroni correction was applied when interpreting statistical significance. Additional analyses were conducted using alternative reference points at ages 4, 5, and 7 years.

Segmented Regression Analysis

To objectively determine and validate the existence of a critical age-related inflection point in dynamics of each parameter, segmented (piece-wise) regression analysis was performed following the method of Muggeo (Muggeo, 2003). According to Muggeo, the initial breakpoint can be determined visually based on the inspection of plotted data (Muggeo, 2003); thus, in this study, a moving-average plot was used to estimate a candidate breakpoint. First, a simple linear regression model was constructed with biopsy age (x_i) as the predictor variable and each parameter as the response variable (y_i), restricting the analysis to patients younger than 11 years ($ABx < 11$ years, $n = 35$) due to insufficient sample size in older age interval (see Results section). Next, segmented regression analysis was performed according to the following model:

$$y_i = \alpha + \beta_1(x_i - \psi)_- + \beta_2(x_i - \psi)_+ + \varepsilon_i, \quad \varepsilon_i \sim N(0, \sigma^2)$$

In this model, α represents the intercept, β_1 and β_2 indicate slopes before and after the breakpoint, respectively, and ψ is the breakpoint (inflection point). The error term (ε_i) was assumed to be normally distributed with a mean of zero and constant variance ($\varepsilon_i \sim N(0, \sigma^2)$). Model improvement introduced by adding the breakpoint was statistically tested using ANOVA, comparing the segmented regression model against the simple linear regression model.

Bayesian Statistical Analysis

Two Bayesian segmented regression analyses were performed. First Bayesian segmented regression was performed using conjugate posterior distribution with the breakpoint fixed at 6.25 years according to the general framework described by

Gelman et al. (Gelman et al., 2025). Model fit was assessed by calculating the Bayesian Information Criterion (BIC) using Schwarz's approximation (Kass and Wasserman, 1995; Volinsky and Raftery, 2000). The ROPE was empirically defined based on measurement errors derived from paired observations between original and ATPase-stained values of the parameter of interest. Furthermore, an additional sensitivity analysis using expanded ROPE ranges (ROPE +1SD, +1.5SD, +2SD) was performed to further examine the stability of the findings.

Second Bayesian segmented regression analysis was conducted using Markov Chain Monte Carlo methods. In this Bayesian model specification, ABx centered at the mean (x_i^*) was modelled as the predictor variable, and the parameter of interest (y_i) as the response variable, defined as follows:

$$y_i = \alpha + \beta_1(x_i^* - \psi^*) + \beta_\Delta(x_i^* - \psi^*) \cdot \text{step}(x_i^* - \psi^*) + \varepsilon_i, \quad \varepsilon_i \sim N(0, \sigma^2)$$

$(\mu x = \text{mean } ABx (<11 \text{ years}); \quad x_i^* = x_i - \mu x, \quad \psi^* = \psi - \mu x)$

Weakly informative priors were selected based on estimates from the frequentist segmented regression. A Bayesian sensitivity analysis was also performed using a ROPE to evaluate whether changes in slopes (β_1, β_Δ) at the estimated breakpoint (ψ^* , defined at zero on centered scale) represented statistically significant differences. Model fit and predictive performance were compared to a simpler linear regression model using leave-one-out information criterion (LOOIC).

Monte Carlo Simulation

Using the LOOCV-derived RMSE as the noise parameter, a Monte Carlo simulation with 2×10^6 draws (chosen so that the binomial standard error for mis-classification probabilities ≤ 0.05 falls below 0.02 percentage points: Monte Carlo Error) converted analytic error into clinical risk by estimating the probability that a histological parameter-based rule would mis-classify patient as younger or older than 6.25 years across hypothetical age gaps of 0.25, 0.50, 0.75, 1.25, 1.25, 1.50, 1.75, and 2.00 years. Moreover, sample-size simulations using Monte Carlo method were conducted to evaluate statistical power for breakpoint detection. Synthetic datasets were generated by randomly sampling age values ($ABx < 11$ years) from observed data with replacement. For each sampled dataset, response values of the parameter of interest were simulated based on estimated segmented regression variables (breakpoint, slopes, and RMSE). Simulations were repeated 10,000 times

for each combination of sample size (20 to 70 in increments of 5) and acceptable error margins (± 1.0 , ± 1.25 , and ± 1.5 years). Breakpoint estimation precision was defined as the proportion of successful estimations (estimated breakpoint within the acceptable margin). Additionally, the second logistic model was inverted to locate the histological parameters' values giving posterior probabilities of 0.80, 0.50 and 0.20 for being <6.25 years; these cut-points defined high-, grey- and low-probability zones that were summarized in a three-level decision table.

Revised Piece-Wise Variance Analysis

To test cross-parameter validity, a group-wise variance analysis was performed. Age strata were defined by the 95% CI of the *MFD* breakpoint: Early ($<\text{CI_low}$), Transitional (CI span) and Late ($\geq\text{CI_high}$). Normality (Shapiro–Wilk) and homogeneity (Levene) directed one-way ANOVA with Tukey, or Kruskal–Wallis with Conover.

Statistical Significance

A significance threshold of significance of $p < 0.05$ was applied to all statistical tests. When interpreting variance analysis results, the primary judgment of statistical significance was based on the mean differences and their 95% CIs. Although effect sizes with their corresponding 95% CIs were essential for assessing the magnitude of differences, statistical significance was not declared if the mean difference's 95% CI crossed zero, even when the 95% CI of the effect size did not. Additionally, unless otherwise specified, "CI" refers to a 95% CI.

Results

Patient Selection

From an initial cohort of 46 muscle biopsy slides, eight were excluded due to severe fading or insufficient tissue, yielding 38 patients aged 1–16 years (**Table 1**); staining methods were not standardized (**Table 2**).

Table 1: Summary of parameters with biopsy year and genotype information

subject	ABx*	Biopsy year	Mean	Cov	Sd	MFD	MFA	Fat	CFA	Genotype†
1	1.0	1983	457.9	0.58	265.7	1471.9	68.9%	0.2%	29.6%	NA
2	1.9	1977	565.3	0.48	271.9	1227.0	72.3%	0.1%	26.7%	NA
3	2.0	1975	622.1	0.53	328.7	1069.5	68.7%	0.2%	30.7%	exon44–47 del
4	2.4	1979	598.1	0.56	336.2	1149.8	71.6%	1.7%	25.8%	exon56 del
5	3.3	1977	851.2	0.54	455.7	656.8	57.3%	0.7%	39.2%	-
6	3.7	1975	531.3	0.44	230.9	953.5	53.7%	0.2%	45.7%	exon44–47 del
7	4.0	1984	1037.9	0.53	551.2	563.2	53.5%	1.3%	41.6%	-
8	4.1	1979	577.5	1.20	693.4	867.2	53.4%	5.3%	40.3%	exon 44–51 del
9	4.3	1973	828.5	0.50	417.0	766.0	65.7%	0.6%	32.1%	exon56 del
10	4.6	1984	870.4	0.65	568.3	545.5	45.9%	1.7%	48.9%	exon44 del
11	4.7	1978	721.1	0.51	365.7	815.2	62.1%	0.8%	36.7%	exon36 del
12	5.0	1980	1007.4	0.50	503.6	571.1	59.5%	1.7%	37.3%	exon43–50 del
13	5.2	1980	624.3	0.53	330.3	976.4	64.9%	0.1%	34.0%	-
14	6.0	1975	725.1	0.82	591.6	552.0	38.5%	1.4%	58.7%	-
15	6.2	1977	1352.0	0.43	585.0	454.7	65.8%	0.1%	31.6%	-
16	6.2	1977	1176.2	1.11	1309.4	365.8	42.2%	1.4%	54.6%	NA
17	6.2	1978	556.3	0.88	489.5	559.9	29.2%	0.7%	67.1%	exon20, exon59 Mut
18	6.3	1979	1602.3	0.78	1244.7	300.7	51.7%	3.5%	44.4%	NA
19	6.4	1979	1520.6	0.95	1442.2	343.8	54.7%	3.1%	40.7%	NA
20	6.5	1979	1554.0	0.61	954.3	400.7	66.8%	0.5%	31.7%	exon6–8 del
21	6.6	1983	1683.7	0.70	1176.0	216.6	36.3%	1.5%	59.9%	-
22	7.0	1978	850.3	0.73	623.7	553.8	47.1%	3.9%	45.3%	-
23	7.2	1979	680.0	0.71	479.3	572.7	39.8%	13.2%	46.6%	exon46–48 del
24	7.2	1976	970.2	0.98	954.0	445.2	45.8%	3.6%	50.2%	NA
25	7.8	1980	772.0	0.60	464.8	458.1	36.4%	6.1%	57.0%	NA
26	8.3	1980	1231.8	1.72	2118.5	245.4	30.4%	6.4%	62.4%	NA
27	8.7	1982	1048.4	1.26	1324.3	497.9	53.9%	0.05%	41.7%	exon50 del
28	8.8	1981	1327.3	0.82	1081.8	282.9	38.6%	3.5%	55.0%	exon3 del
29	8.9	1979	613.6	0.86	526.5	386.5	23.5%	18.6%	55.9%	-
30	9.1	1982	1285.4	0.95	1215.0	423.0	59.0%	5.0%	33.6%	exon44 del
31	9.7	1976	889.0	0.75	666.2	291.0	25.4%	3.2%	68.2%	-
32	9.8	1982	1203.7	0.78	943.5	414.1	52.8%	8.6%	37.3%	exon51–60 del
33	10.3	1980	3643.5	0.99	3603.9	143.9	58.2%	10.3%	30.8%	exon12 dupl
34	10.7	1982	909.6	0.90	821.4	240.5	20.8%	6.0%	71.6%	exon44 del
35	10.9	1977	1565.2	0.77	1199.8	393.5	67.7%	3.0%	28.7%	exon56 del
36	12.8	1983	1028.5	1.07	1096.0	219.3	20.9%	3.4%	73.7%	NA
37	15.1	1973	1953.9	0.92	1787.6	170.2	33.9%	9.4%	54.6%	NA
38	16.3	1973	1504.0	1.46	2189.0	172.1	26.5%	15.4%	55.9%	exon46–49 del

(Abbreviations: *ABx*, age at biopsy; *Mean*, mean myofiber size; *Sd*, standard deviation of myofiber size; *Cov*, coefficient of variation of myofiber size; *MFD*, myofiber density; *MFA*, myofiber area; *Fat*, fatty degeneration area; *CFA*, connective/fibrotic tissue area; del, deletion; Mut, mutation; dupl, duplication; MLPA, multiplex ligation-dependent probe amplification; PCR, polymerase-chain reaction; NA, not available.)

* *ABx* was treated as a continuous variable in correlation analyses and is reported to one decimal place. For analytical precision, exact age was determined by incorporating the month of biopsy, determined by dividing a year into 12 and adding the resulting fraction to the *ABx*. For patients with identical age and month values, ranking was further refined by accounting for the number of weeks.

† Genetic mutations were identified via MLPA or PCR. "NA" denotes patients who did not undergo genetic testing, whereas a hyphen (-) indicates cases in which no mutation was identified despite testing.

Table2: The availability of sample for semi-quantitative image analysis

Subject	Frozen H&E	Frozen G-T	FFPE H&E	FFPE M-T	Frozen ATPase
1	○	○	×	×	○
2	○	○	×	×	×
3	×	×	○	○	×
4	○	○	○	×	○
5	○	○	×	×	×
6	×	×	○	○	×
7	○	○	×	×	○
8	○	○	×	×	×
9	○	○	○	○	×
10	○	○	×	×	×
11	○	○	○	○	×
12	○	○	×	×	○
13	○	○	×	×	○
14	×	×	×	○	×
15	○	○	×	×	×
16	○	○	×	○	×
17	×	×	○	×	×
18	○	○	×	×	×
19	○	○	×	×	○
20	○	○	×	×	○
21	○	○	×	×	○
22	○	○	×	×	×
23	○	○	×	×	×
24	○	×	×	×	×
25	○	○	×	×	×
26	○	○	×	×	×
27	○	○	×	×	×
28	○	○	○	○	×
29	○	○	×	×	○
30	×	○	×	×	○
31	○	○	×	×	×
32	○	○	×	×	○
33	○	○	×	×	○
34	×	○	×	×	○
35	○	○	×	×	×
36	○	○	×	×	×
37	×	○	×	×	×
38	×	○	×	×	○

(**Abbreviations:** FFPE, formalin-fixed paraffin-embedded; H&E, hematoxylin-eosin; G-T, Gomori Trichrome; M-T, Masson Trichrome; ATPase, actomyosin adenosine triphosphatase.)

○: available; ×: severe fading, insufficient tissue quantity, or loss.

Comparison between H&E and G-T Staining Methods

To briefly supplement the description in the Materials and Methods section prior to presenting these results, at the time of this comparison, specimen collection and validation were still at an early stage, and the full set of biopsy samples had not yet been assembled. Consequently, to address methodological concerns regarding staining variability, a preliminary evaluation was performed on a limited subset of available paired specimens to determine whether different staining methods (H&E and G-T) could reliably be integrated in subsequent quantitative analyses. On this basis, in the preliminary analysis of 16 paired specimens, no significant difference in *MFA* values between H&E and G-T staining was observed (Wilcoxon signed-rank test, $p > 0.05$). Power analysis indicated that approximately 28 pairs would yield sufficient statistical power (80%). Thus, the sample size was increased to 28 paired specimens. Once again, no significant differences were found between *MFA* measurements from H&E- and G-T-stained slides (Wilcoxon signed-rank test, $p \approx 0.9$; Cliff's $\delta = 0.015$ [CI -0.28 , 0.31], negligible). Subsequent power analysis revealed that detecting any significant differences would require an impractically large sample size (approximately $n = 450$), further suggesting negligible practical differences between the two staining methods. Additionally, Pearson's product-moment correlation coefficient demonstrated an extremely strong correlation between *MFA* values obtained from H&E and G-T staining methods ($r = 0.97$, $p < 0.001$; **Figure 2**), confirming statistical interchangeability based on the interpretation described by Bell and Conen (Bell and Conen, 1967). Validation using *CFA* was omitted because *MFA* and *CFA* showed a statistically significant and extremely strong correlation in the main correlation analysis (Pearson's $r = 0.96$).

Bayesian approach showed that approximately 82% of the posterior for the standardized difference lay inside the ROPE (posterior Cohen's $d = 0.12$, 95% Highest Density Interval = -0.26 to 0.49). The BF_{10} favored the null hypothesis ($BF_{10} = 0.101$), showing substantial (almost strong) evidence according to the Jeffreys' criteria (Kass and Raftery, 1995). Mixed-effects modeling further demonstrated negligible specimen-level variance attributable to staining differences (variance reduction = 0.03%).

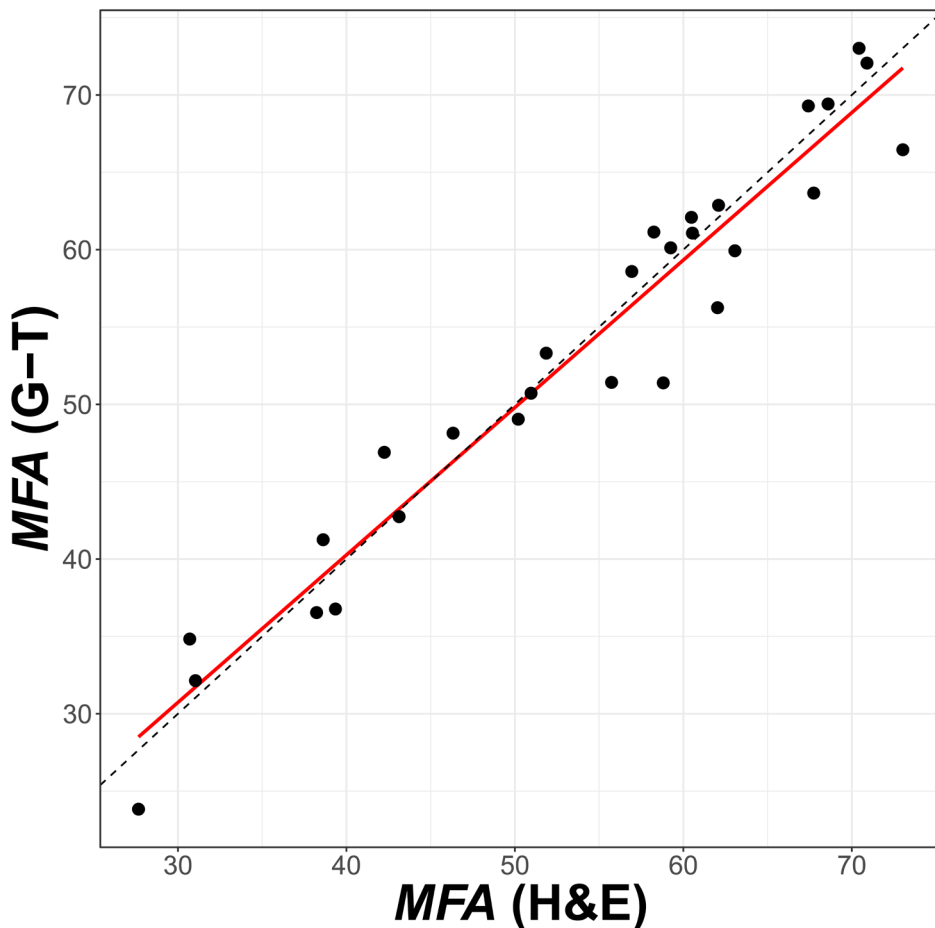


Figure 2: Correlation of *MFA* between H&E- and G-T-stained samples

The horizontal and vertical axes represent *MFA* values (%) from H&E- and G-T-stained slides, respectively. Pearson's product-moment correlation coefficient (*r*) between *MFA* values obtained from 28 pairs of matched H&E- and G-T-stained slides was approximately 0.97.

(Abbreviations: *MFA*, myofiber area; H&E, hematoxylin-eosin; G-T, Gomori trichrome.)

Histopathological Findings

Histological evaluation revealed distinct differences in *MFD* patterns between specimens obtained from patients younger than 6 years and those from older age groups, as described in subsequent sections. The majority of samples exhibited histopathological alterations, including MFS variation, the presence of hypercontracted myofibers and internally nucleated myofibers, increase of connective tissue, reduced *MFA*, widened inter-myofiber spacing, and adipose tissue replacement (Figure 3).

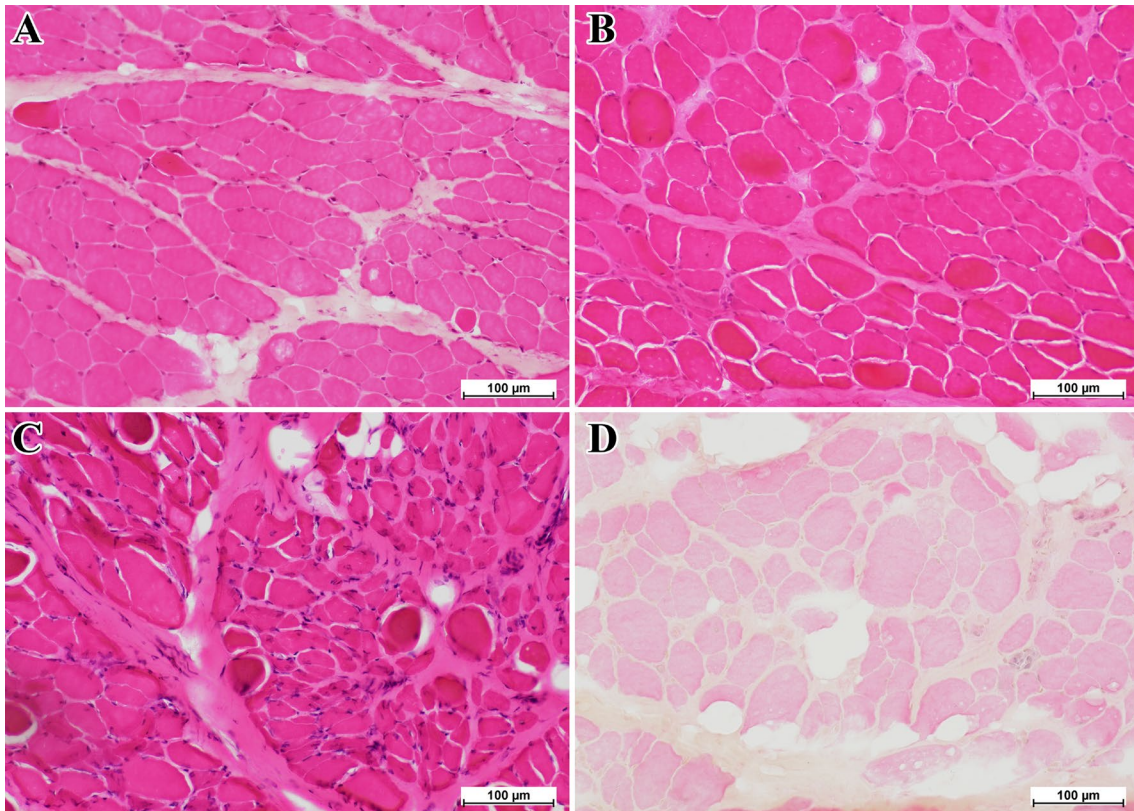


Figure 3: Representative H&E-stained images of DMD patients at different ages

Each panel presents representative H&E-stained microphotographs obtained from patients of specific ages (200 \times magnification for each): 4 years and 4 months (**A**), 6 years and 2 months (**B**), 7 years and 0 months (**C**), and 9 years and 9 months (**D**). Note that the FOI corresponded to a 10 \times objective lens, although all panels are displayed at 20 \times objective lens.

A: In the 4-year-old patient, myofibers exhibit uniform histological findings with well-preserved *MFA* and an increased area of connective tissue.

B: The 6-year-old patient similarly exhibits uniform myofibers with comparable *MFA* to panel A; however, a remarkable *MFD* reduction is observed upon quantification.

Comparison of panels A and B shows *MFA* values of 65.69% and 65.77%, respectively, while *MFD* values decline from 765.96 to 454.67. Connective tissue area is further increased, with *CFA* values of 32.06% and 31.55% in panels A and B, respectively.

C: In the 7-year-old patient, increased MFS variability is evident, accompanied by pronounced increased area of connective tissue and the mild fat invasion emergence.

D: The 9-year-old patient exhibits significant reductions in both *MFD* and *MFA*, accompanied by remarkable increase of connective tissue and localized fat replacement area.

(Abbreviations: DMD, Duchenne muscular dystrophy; H&E, hematoxylin-eosin; FOI, field of interest; LUTs, look-up tables; *MFA*, myofiber area; *MFD*, myofiber density; *CFA*, connective/fibrotic tissue area; *MFS*, myofiber size.)

Correlation between Age and Histological Parameters

To identify new pathological metrics, correlations between *ABx* and key histological parameters were assessed. All selected variables contained complete datasets. The results of image-based quantitative analyses are presented in **Table 1**, alongside biopsy year and genotype data. Among all parameters, *MFD* exhibited the strongest correlation with *ABx*, demonstrating a marked decline between 1 and 6 years (**Figure 4**). Spearman's correlation coefficients for key variables were as follows: *Mean* (rho = 0.61), *Sd* (rho = 0.74), *Cov* (rho = 0.66), *MFD* (rho = -0.85), *MFA* (rho = -0.60), *Fat* (rho = -0.69), *CFA* (rho = -0.48), and *Opaque* (rho = 0.34) (**Figure 4**). No statistically significant correlations were observed for *ABx* with *IntN*, *NFA*, and *RFA*.

Due to the observed non-linear correlation, particularly evident between *MFD* and *ABx*, standard linear modeling did not adequately result in reflecting the complexity of these relationships. All parameters initially demonstrated significant variability and skewness, particularly *MFD*, which exhibited clearly non-linear distributions across *ABx*. Following data preprocessing, transformed parameters as described in the Materials and Methods section demonstrated clearly stabilized variances and markedly reduced skewness, resulting in notably improved linear relationships. This enhancement was particularly evident in the correlation between *ABx* and transformed *MFD*, where previously pronounced non-linearities were significantly alleviated, thus confirming the necessity of the transformation.

After these transformations, Pearson's product-moment correlation coefficients confirmed strong linear associations between *ABx* and key parameters (e.g., *MFD*: $r = -0.86$). Consequently, parameters verified by these statistical assessments formed the basis for the subsequent multiple regression modeling, and also guided the selection of candidate variables employed in the stepwise regression approach as described in the next paragraph.

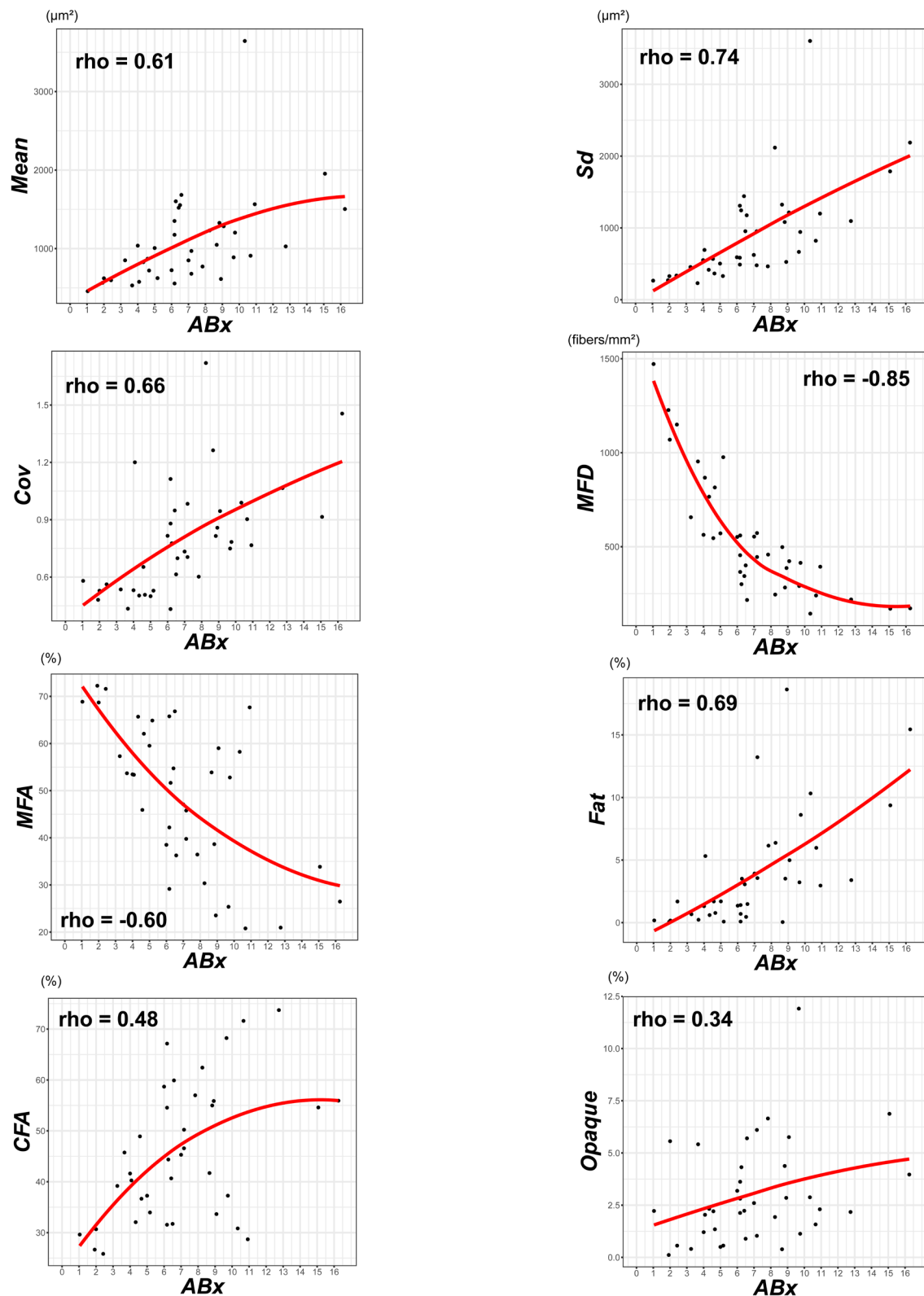


Figure 4: Correlation analysis

Scatter plots illustrate the relationships between *ABx* and each parameter shows a statistically significant correlation, with Spearman's correlation coefficients (*rho*)

indicated. Red line is an approximate curve (R setting: span = 2, except for *MFD* (1)).
(Abbreviations: *ABx*, age at biopsy; *Mean*, mean myofiber size; *Sd*, standard deviation of myofiber size; *Cov*, coefficient of variation of myofiber size; *MFD*, myofiber density; *MFA*, myofiber area; *CFA*, connective/fibrotic tissue area; *Fat*, fatty degeneration area; *Opaque*, percentage of opaque fibers relative to *MFD*.)

Multiple Regression Analysis

Based on the results of the correlation analyses, several candidate variables (transformed as described earlier) were detected: *Mean*, *Cov*, *Sd*, *MFD*, *MFA*, *CFA*, and *Fat*. Subsequent multiple regression analyses with stepwise selection excluded *Fat* due to a lack of significant predictive contribution. As a result, two robust regression models were established for predicting *ABx*. The first model including *MFD* and its interaction term with *Sd* yielded an adjusted R^2 of 0.79 (**Figure 5**).

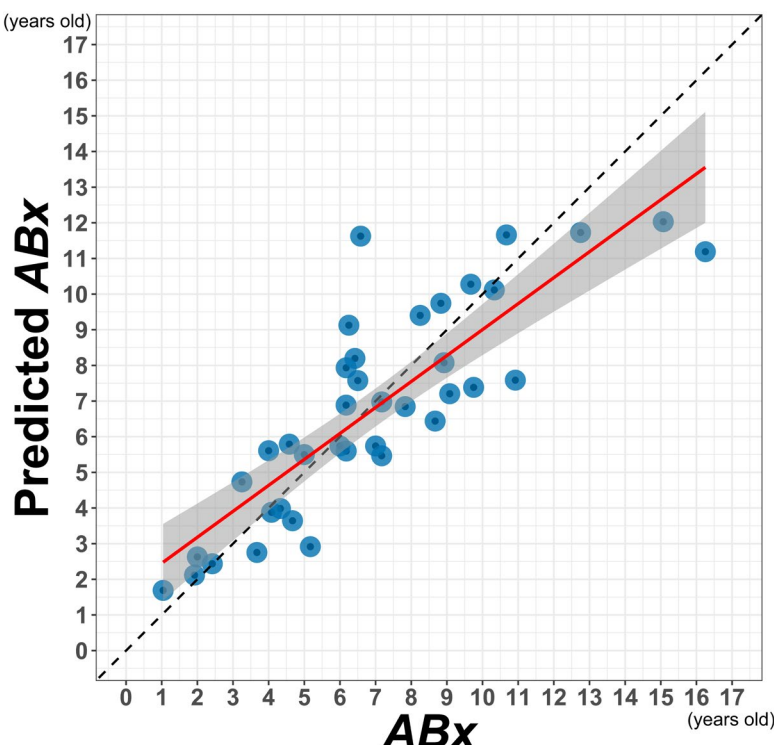


Figure 5: Age-prediction model established by multiple regression analysis

An age-prediction plot was constructed using a multiple regression model with *ABx* as the dependent variable and *MFD* and the interaction term (*MFD* and *Sd*) as predictors. As described in the main text, this model explained approximately 80% of the total variance in the predicted *ABx*. The gray area indicates the standard error.

(Abbreviations: *ABx*, age at biopsy; *MFD*, myofiber density; *Sd*, standard deviation of myofiber size.)

In this model, the standardized coefficient for *MFD* was -0.87 [CI -1.03 , -0.72] and the interaction term between standardized *MFD* and *Sd* was 0.21 [CI 0.080 , 0.35]; both terms were statistically significant. The second model including *MFD* and its interaction term with *Mean* yielded an adjusted R^2 of 0.80 . The general variance inflation factors confirmed the absence of multicollinearity among explanatory variables. Additionally, the significance of the interaction terms was verified through incremental *F*-tests comparing models with and without the interaction terms ($p < 0.01$). AIC was 53.84 . Diagnostic plots indicated that the first model had superior residual normality and fewer influential outliers (all Cook's distances <0.50 ; **Figure 6**). The LOOCV for this model yielded an RMSE of 0.49 , with a SD of 0.32 .

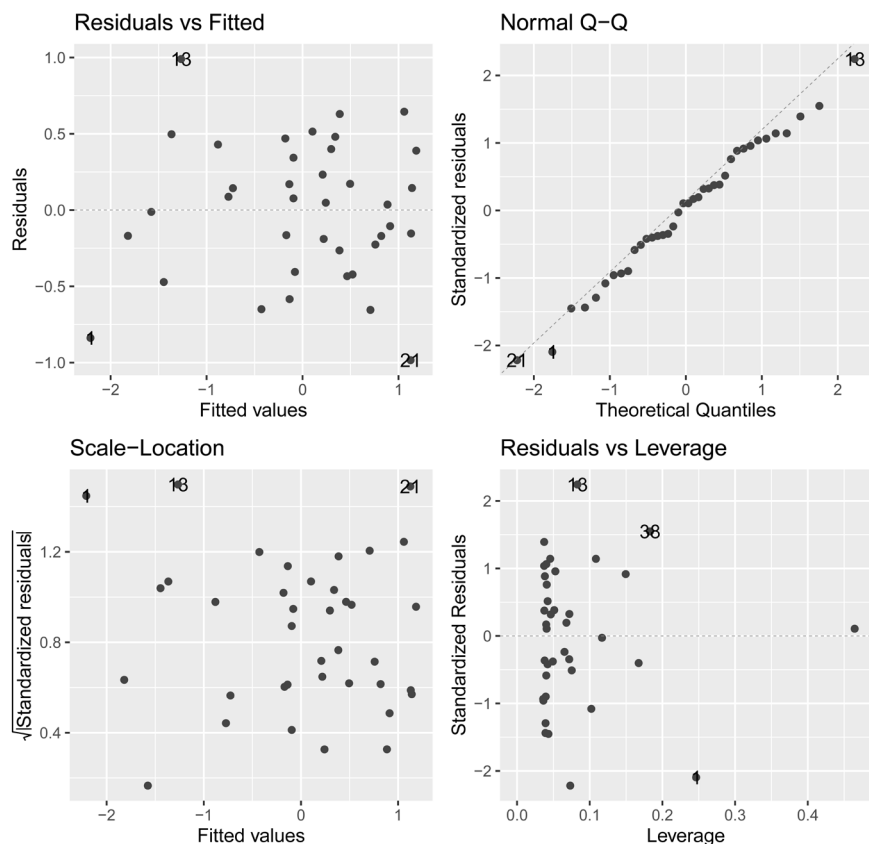


Figure 6: Diagnostic plots for the first multiple regression model

Model diagnostics to evaluate the validity of regression assumptions are shown. The multiple regression model included *ABx* as the dependent variable, and *MFD* and its interaction with *Sd* as predictors.

(Abbreviations: *ABx*, age at biopsy; *MFD*, myofiber density; *Sd*, standard deviation of myofiber size.)

A Kruskal–Wallis test for prediction errors of the first regression model across predefined detailed age groups showed significant differences among the specified age groups (**Figure 7**).

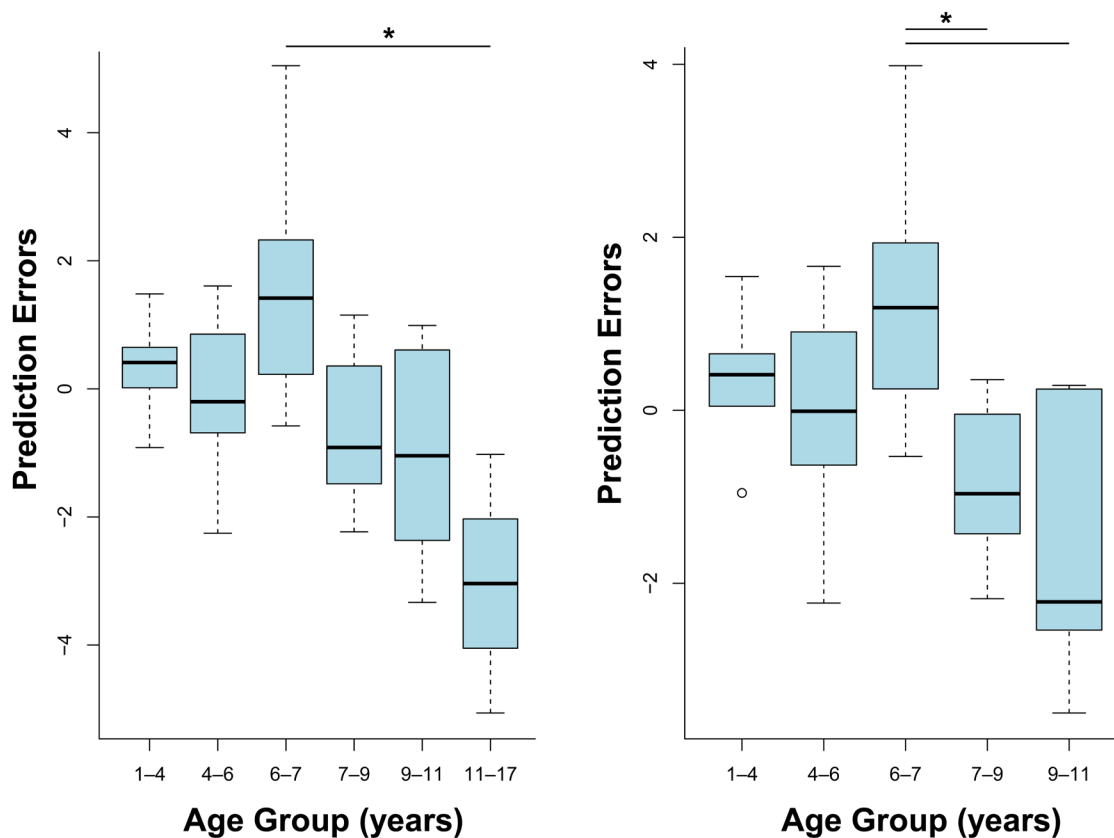


Figure 7: Box plot of residual (predictive error) values

Using the difference between predicted and actual *ABx* as a variable, an inter-group comparison was performed using the Kruskal–Wallis test (due to the limited sample size ($n = 3$) in the 11–17 years age group). The post-hoc test revealed statistically significant differences among age groups ($p < 0.05$; asterisks (*) denote statistical significances).

(Abbreviation: *ABx*, age at biopsy.)

Specifically, error analysis showed that prediction errors were minimized when patients were limited to those younger than 7 years old, whereas prediction accuracy significantly declined in older age groups (**Figure 8**).

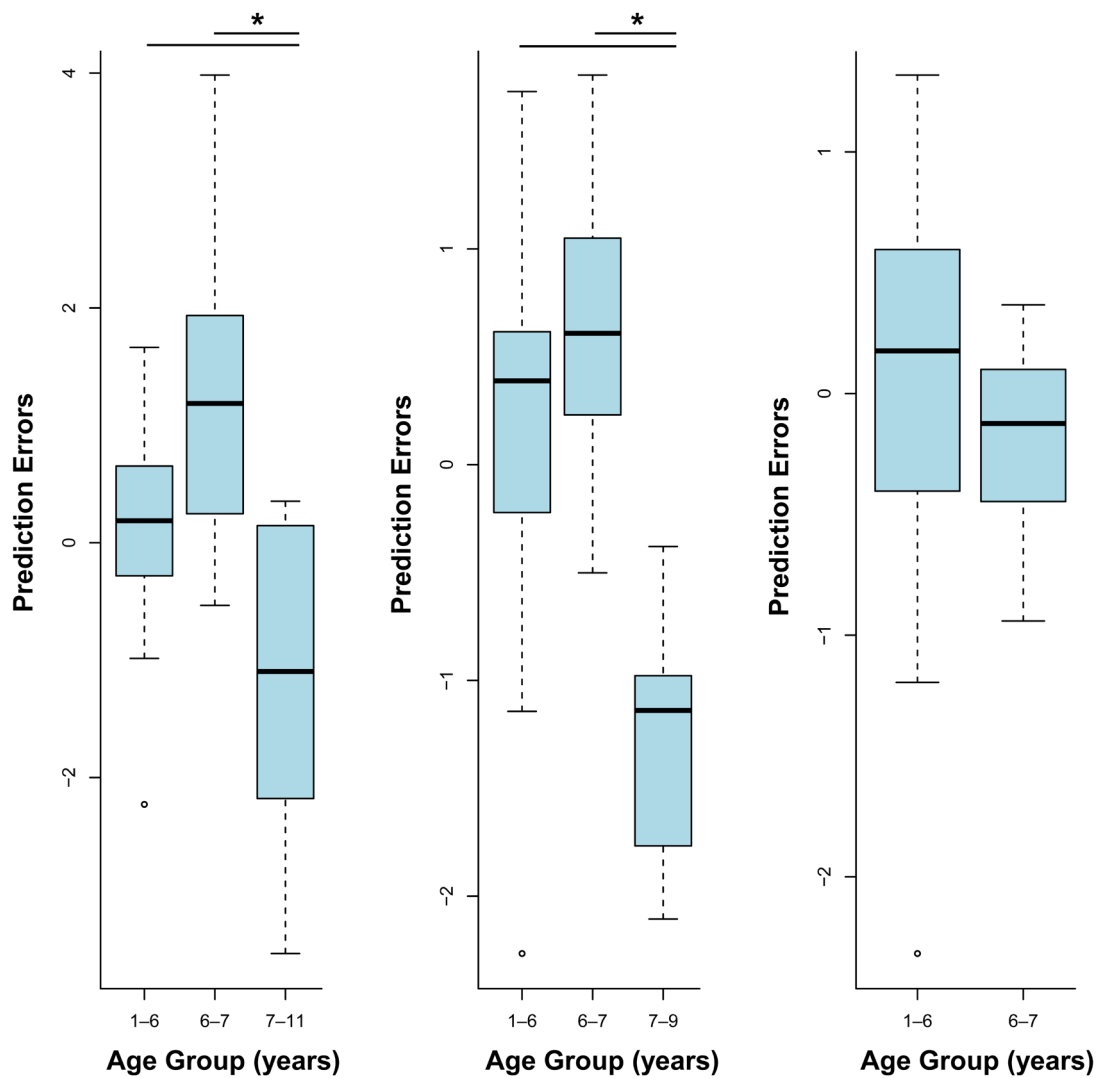


Figure 8: Distribution of prediction errors across different age groups

Boxplots demonstrate prediction errors (the differences between predicted and actual *ABx*) stratified by re-specified age intervals. Statistical comparisons were performed using the Kruskal–Wallis test for three-group analyses (left and center) and Wilcoxon rank-sum test for two-group analysis (right). The post-hoc Conover tests showed significant differences across groups 1–6, 6–7, and 7–11 years (left panel; $p < 0.01$), and similarly significant results were found for age groups 1–6, 6–7, and 7–9 years (center panel; $p < 0.01$). Asterisks (*) denote statistical significances. Conversely, comparison between age groups 1–6 and 6–7 years (right panel) showed no statistically significant difference ($p = 0.30$), with a small effect size as indicated by Cliff's δ of 0.288 [CI $-0.24, 0.69$].

(Abbreviations: *ABx*, age at biopsy; CI, Confidence interval.)

Accordingly, in a multiple regression model restricting the sample to patients aged under 7 years (including *MFD* and its interaction with *Sd*; **Figure 9**), both predictors remained statistically significant, showing an improved model fit (adjusted $R^2 = 0.75$, AIC = 29.12) and a comparable predictive accuracy (RMSE = 0.47, SD = 0.38) validated by LOOCV.

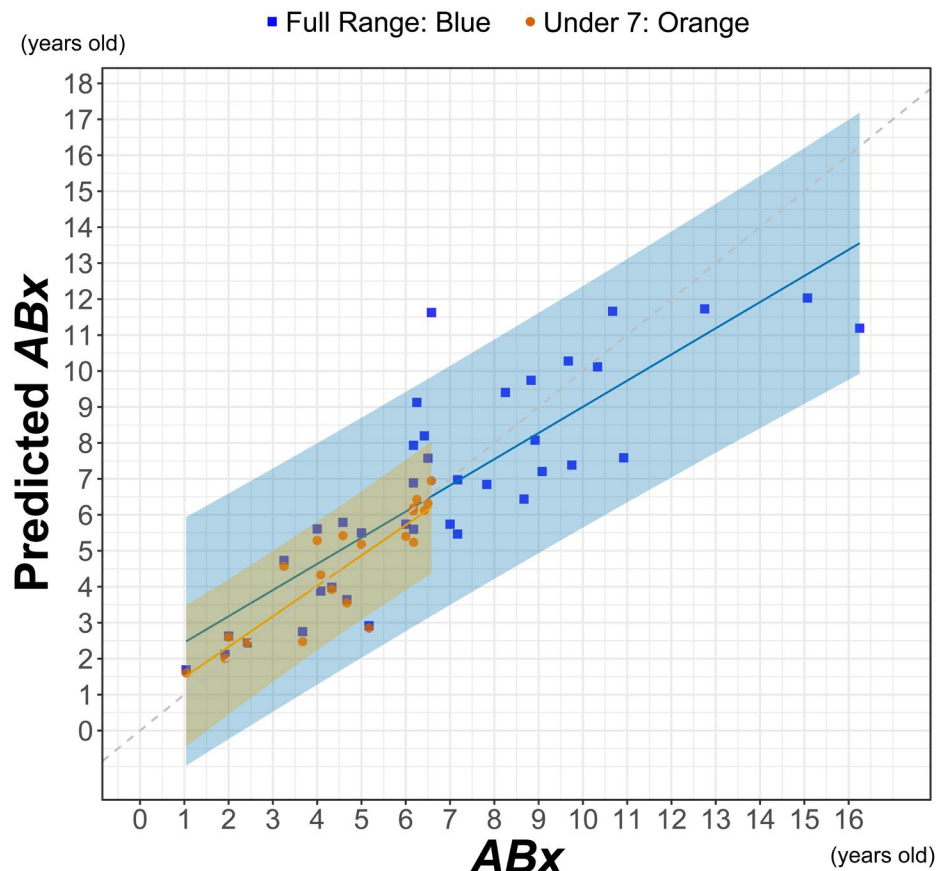


Figure 9: Comparison of predicted *ABx* from two multiple regression models
Scatter plot comparing predicted versus actual *ABx* from two separate multiple regression analyses: a model based on the full dataset (38 samples, indicated by blue squares and blue regression line with CI shaded blue), and a model restricted to patients younger than 7 years (21 samples, indicated by orange dots and orange regression line with CI shaded orange). The narrower CI of the predicted *ABx* values in the restricted dataset corresponds to the reduced prediction error per individual case compared with the model using the full age range. The dotted line represents perfect prediction accuracy ($y = x$).

(**Abbreviations:** *ABx*, age at biopsy; CI, confidence interval.)

Age-Related Variability in Histological Parameters

To further delineate age-related histopathological changes, patients were stratified into four age cohorts based on the report by Peverelli et al. (Peverelli et al., 2015) and the preliminary data obtained via multiple regression analysis and error analysis as described earlier: 1–6 years ($n = 13$), 6–7 years ($n = 8$), 7–11 years ($n = 14$). Statistically significant differences in *Mean*, *Sd*, *Cov*, *MFD*, and *CFA* were observed between the 1–6 and 6–7 age groups (**Figure 10A, Table 2**). Comparisons between the 1–6 and 7–11 age groups showed statistically significant differences across most parameters (**Figure 10A, Table 3**), with the exception of *IntN*, *NFA*, *RFA*, and *Opaque*. Notably, in the box plot analysis, *MFD* exhibited the greatest variability within the 1–6-year cohort, whereas the *Cov* had the narrowest interquartile-range (0.50–0.56) within this same group (**Figure 10A, Table 3**).

Based on the above results, additional effect sizes were calculated using Hedges' *d* with bootstrapped CI for *Mean*, *Sd*, and *Cov* after excluding extreme outliers affecting normality assumptions (*Mean* and *Sd*: age group 7–11; *Cov*: age groups 1–6 and 7–11). After exclusion, normality assumptions were met for these parameters in the specified age groups, yielding the same statistical significances corresponding to the original findings (**Table 4**).

Age-Stratified MFD Distributions

Although exploratory due to the relatively small sample sizes per group, additional box plots were generated to further elucidate age-related variations in *MFD*, categorizing patients into the following age groups: 1–4 years ($n = 6$), 4–6 years ($n = 7$), 6–7 years ($n = 8$), 7–9 years ($n = 8$), and 9–11 years ($n = 6$) (**Figure 10B**). Notably, the minimum values and first quartiles within the 4–6-year age group overlapped with the maximum values observed in the 6–7 and 7–9 groups (**Table 5**).

In any case, among all parameters, *MFD* exceptionally demonstrated near-complete separation in the box plot analyses. Additionally, further comparisons were conducted between the aggregated age groups: the first comparison contrasts *MFD* distributions between the age groups 1–6 ($n = 13$) vs 6–11 ($n = 22$) years, and the second comparison contrasts age groups 1–7 ($n = 21$) vs 7–11 ($n = 14$) years (**Figure 10C**). These plots visually delineated an *MFD* threshold range of approximately 500–600, which subsequently served as the foundation for logistic regression modeling.

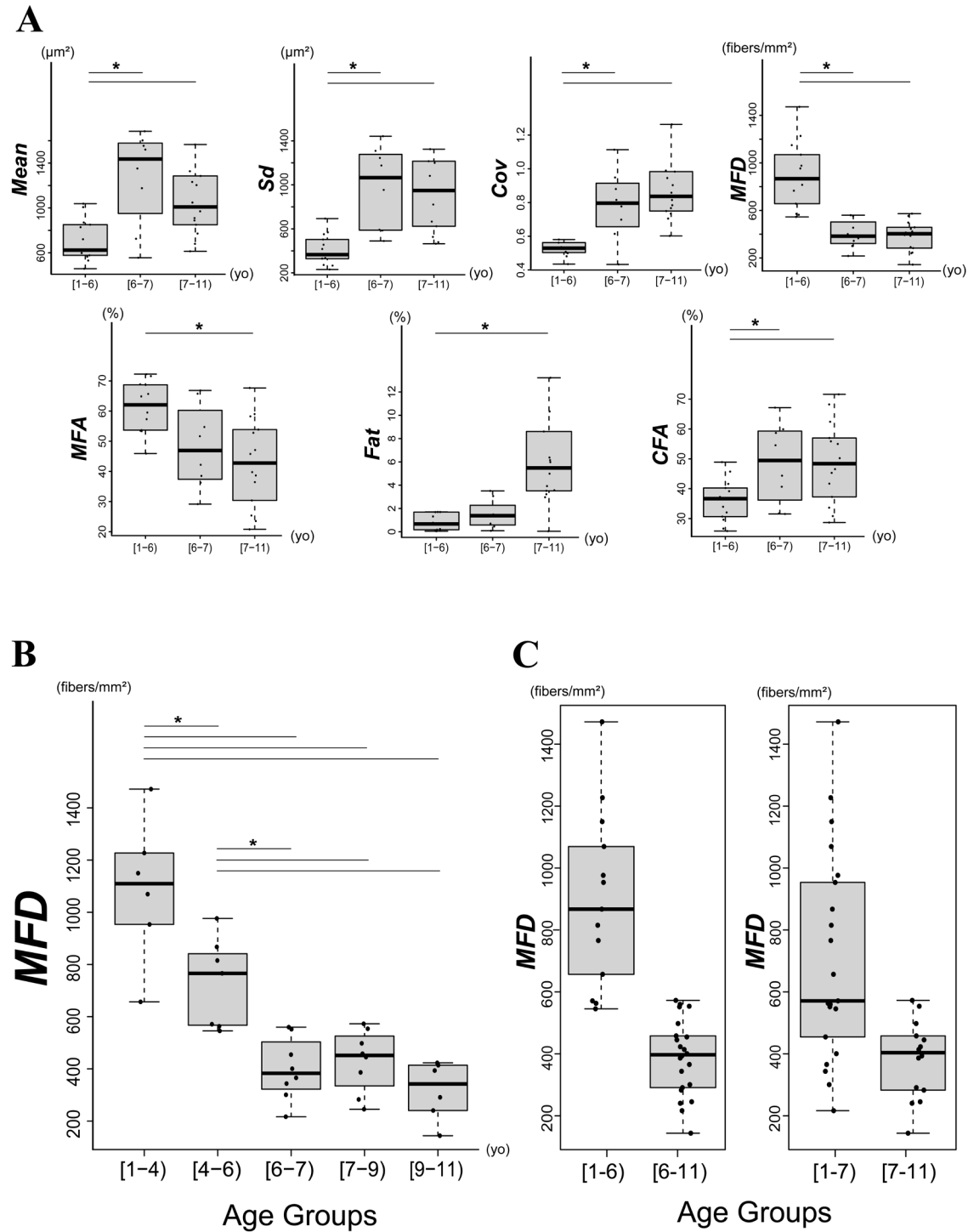


Figure 10: Box plot analyses across age groups

A: Box plots illustrate the results of variance analyses and corresponding post-hoc comparisons for multiple morphological parameters: *Mean*, *Sd*, *Cov*, *MFD*, *MFA*, *Fat*, and *CFA*. Data are stratified by three specific age groups: 1–6, 6–7, and 7–11 years. Each parameter is displayed in a separate panel to facilitate direct visual comparison

among age groups. The age groups are denoted using the interval notation [X, Y), indicating that each range includes ages greater than or equal to X and strictly less than Y. Statistical comparisons between groups were performed using ANOVA, Welch's ANOVA, and Kruskal–Wallis test. Following these analysis, post-hoc Tukey's HSD test, Games–Howell test, or Conover test with Bonferroni correction were applied for pairwise comparisons to determine which specific age groups significantly differed from each other. Statistically significant differences identified by these pairwise comparisons are indicated by asterisks (*). Outliers, defined as data points exceeding the $1.5 \times$ interquartile-range from the quartiles, are not displayed in the plots to maintain visual clarity but were included in all statistical analyses and calculations. These parameters show a quantitative characterization across the age spectrum. In patients within the youngest age group (1–6 years), the variability in parameters related to MFS (*Mean* and *Sd*) as well as MFS heterogeneity (*Cov*) is limited. In contrast, *MFD* values show a wider distribution.

B: A refined box plot of *MFD* presents a more granular age stratification (1–4, 4–6, 6–7, 7–9, and 9–11 years), where asterisks (*) denote statistically significant differences between age groups, consistent with panel A. Statistical significance was assessed by first verifying normality and homogeneity of variances using the Shapiro-Wilk and Levene's tests, respectively. ANOVA, followed by the post-hoc Tukey's HSD test, was then conducted to compare groups. For each pairwise comparison, the mean difference and its 95% CI were calculated to determine statistical significance.

C: This panel presents box plots of *MFD* data using two distinct age stratifications for comparative visualization. Specifically, two separate comparisons are depicted: the first comparison contrasts *MFD* distributions between the age groups 1–6 vs 6–11 years, and the second comparison contrasts age groups 1–7 vs 7–11 years. These box plot analyses show two distinct distribution patterns of *MFD* data associated with different age thresholds.

(**Abbreviations:** MFS, myofiber size; *Mean*, mean MFS; *Sd*, standard deviation of MFS; *Cov*, coefficient of variation of MFS; *MFD*, myofiber density; *MFA*, myofiber area; *CFA*, connective/fibrotic tissue area; *Fat*, fatty degeneration area; ANOVA, analysis of variance; CI, confidence interval.)

Table 3: Variance analysis and post-hoc test results

	Comparison	Effect size [95% CI]	Mean difference [95% CI]	Required sample [§]
<i>Mean</i> [*]	1–6 vs 6–7 years	0.69 [0.19, 1.00]	556.43 [225.90, 886.96]	8.62
	1–6 vs 7–11 years	0.68 [0.35, 0.92]	498.73 [72.66, 924.80]	8.96
	6–7 vs 7–11 years	-0.29 [-0.80, 0.29]	-57.70 [-578.73, 463.33]	59.53
<i>Sd</i> [*]	1–6 vs 6–7 years	0.88 [0.65, 1.00]	564.96 [276.94, 852.98]	4.37
	1–6 vs 7–11 years	0.86 [0.63, 0.99]	735.35 [270.39, 1200.30]	4.83
	6–7 vs 7–11 years	-0.054 [-0.57, 0.45]	170.38 [-369.44, 710.21]	1739.43
<i>Cov</i> [*]	1–6 vs 6–7 years	0.60 [0.039, 1.00]	0.20 [0.013, 0.40]	12.3
	1–6 vs 7–11 years	0.86 [0.56, 1.00]	0.34 [0.14, 0.53]	4.83
	6–7 vs 7–11 years	0.21 [-0.32, 0.68]	0.13 [-0.090, 0.35]	107.15
<i>MFD</i> [†]	1–6 vs 6–7 years	-1.75 [-2.85, -1.25]	-495.60 [-682.45, -308.75]	6.27
	1–6 vs 7–11 years	-1.81 [-2.91, -1.35]	-512.81 [-689.04, -336.58]	5.94
	6–7 vs 7–11 years	-0.14 [-1.24, 0.92]	-17.21 [-129.64, 95.21]	753.79
<i>MFA</i> [‡]	1–6 vs 6–7 years	-1.19 [-2.65, -0.33]	-13.20 [-26.86, 0.48]	12.13
	1–6 vs 7–11 years	-1.51 [-2.56, -0.86]	-18.52 [-30.24, -6.80]	8.01
	6–7 vs 7–11 years	-0.36 [-1.28, 0.46]	-5.33 [-18.82, 8.16]	123.40
<i>Fat</i> [*]	1–6 vs 6–7 years	0.25 [-0.23, 0.71]	0.39 [-0.82, 1.61]	78.28
	1–6 vs 7–11 years	0.79 [0.44, 1.00]	5.42 [2.64, 8.20]	6.10
	6–7 vs 7–11 years	0.80 [0.46, 1.00]	5.03 [2.19, 7.87]	5.84
<i>CFA</i> [†]	1–6 vs 6–7 years	1.77 [0.44, 3.87]	12.54 [1.78, 23.31]	6.14
	1–6 vs 7–11 years	1.81 [0.77, 3.71]	12.85 [4.35, 21.35]	5.91
	6–7 vs 7–11 years	0.023 [-1.08, 1.06]	0.31 [-12.17, 12.78]	29960.25

(**Abbreviations:** CI, confidence interval; NS, not significant; ANOVA, analysis of variance; *Mean*, mean myofiber size; *Sd*, standard deviation of myofiber size; *Cov*, coefficient of variation of myofiber size; *MFD*, myofiber density; *MFA*, myofiber area; *Fat*, fatty degeneration area; *CFA*, connective/fibrotic tissue area.)

*Cliff's δ for variables violating normality assumptions (*Mean*, *Sd*, *Cov*, and *Fat*).

[†] Glass's Δ for variables with unequal variances (*MFD* and *CFA*).

[‡] Hedges' d for normally distributed variable with equal variances (*MFA*).

[§] The per-group sample size required to detect the observed effect with 80% power.

Table 4: Additional effect size analyses excluding extreme outliers

	Comparison	Effect size [95% CI]
<i>Mean</i> [†]	1–6 vs 6–7 years	1.81 [0.79, 4.70]
	1–6 vs 7–11* years	1.27 [0.61, 2.26]
	6–7 vs 7–11* years	−0.69 [−2.18, 0.22]
<i>Sd</i> [†]	1–6 vs 6–7 years	2.15 [1.32, 4.43]
	1–6 vs 7–11* years	1.57 [1.10, 2.70]
	6–7 vs 7–11* years	−0.042 [−1.08, 0.71]
<i>Cov</i> [‡]	1–6* vs 6–7 years	1.79 [0.81, 4.24]
	1–6* vs 7–11* years	2.47 [1.87, 4.28]
	6–7 vs 7–11* years	0.36 [−0.60, 1.31]

(Abbreviations: CI, confidence interval; *Mean*, mean myofiber size; *Sd*, standard deviation of myofiber size; *Cov*, coefficient of variation of myofiber size.)

*Age groups including extreme outliers.

[†] For *Mean* and *Sd*, data from subject 33 were excluded.

[‡] For *Cov*, data from subjects 8 and 26 were excluded. Although the original effect size analysis for *Cov* between the 1–6 and 6–7 age groups had a CI crossing zero, this was resolved upon exclusion of the specified outliers.

Table 5: Quartile summary of *MFD* across the detailed age groups

Age group	Min.	1st Qu.	Median	Mean	3rd Qu.	Max.
1–4 years	656.84	982.48	1109.62	1088.09	1207.73	1471.93
4–6 years	545.49*	567.15*	765.96	729.22	841.22	976.36
6–7 years	216.62	332.99	383.21	399.26	479.00	559.89*
7–9 years	245.37	360.62	451.66	430.31	511.88	572.69*
9–11 years	143.94	253.14	342.28	317.69	408.97	423.02

(Abbreviation: *MFD*, myofiber density.)

*The minimum value and first quartile within the 4–6-year age group overlapped with the maximum values observed in the 6–7 and 7–9 groups.

MFD Thresholds in Logistic Regression Analysis

To identify critical *MFD* thresholds associated with age 6, a series of logistic regression models were developed, evaluating thresholds within the 500–600 range. Several thresholds achieved statistical significance, demonstrating low AIC values, high classification accuracy, and markedly low ORs (**Table 6**). Specifically, *MFD* thresholds between 546 and 551 demonstrated statistical significance (AIC = 29.83, accuracy = 85.71%, OR = 0.019 [CI 0.00087, 0.13]), as did thresholds of 552–553 (AIC = 26.95, accuracy = 88.57%, OR = 0.013 [CI 0.00059, 0.099]) and 554–559 (AIC = 25.27, accuracy = 91.43%, OR = 0.0083 [CI 0.00034, 0.070]). The most robust findings were observed for thresholds between 560 and 563, which yielded the lowest AIC value (19.19), the highest classification accuracy (94.29%), and an exceptionally low OR (0.0040 [CI 0.00010, 0.043]). Thresholds of 564–571 (AIC = 24.47, accuracy = 91.43%, OR = 0.0087 [CI 0.00035, 0.074]) and the discrete threshold of 572 (AIC = 28.79, accuracy = 88.57%, OR = 0.014 [CI 0.00064, 0.11]) retained statistical significance.

However, the *p*-value for the *MFD* threshold of 546–551 fibers/mm² slightly exceeded the Bonferroni-corrected significance level of 0.000495, and *MFD* thresholds within the 500–545 and 573–600 ranges failed to achieve statistical significance (**Table 6**). Additional analyses incorporating alternative critical ages (4, 5, or 7 years) identified statistically significant *MFD* thresholds; however, these thresholds encompassed broader ranges compared with those identified at age 6. The reference age used in this logistic regression analysis was subsequently employed as the initial breakpoint in the segmented regression analysis performed next, based on the results described above.

Table 6: Logistic regression analysis results for patients < 6 years and ≥ 6 years

<i>MFD</i> threshold (fibers/mm²)	AIC	Accuracy	OR [95% CI]
500–545	22.55	88.57%	NS
546–551* (<i>p</i> = 0.00071)	29.83	85.71%	0.019 [0.00087, 0.13]
552, 553 (<i>p</i> <0.000495)	26.95	88.57%	0.013 [0.00059, 0.099]
554–559 (<i>p</i> <0.000495)	25.27	91.43%	0.0083 [0.00034, 0.070]
560–563 (<i>p</i> <0.000495)	19.19	94.29%	0.0040 [0.00010, 0.043]
564–571 (<i>p</i> <0.000495)	24.47	91.43%	0.0087 [0.00035, 0.074]
572 (<i>p</i> <0.000495)	28.79	88.57%	0.014 [0.00064, 0.11]
573–600	22.35	91.43%	NS

(**Abbreviations:** AIC, Akaike's information criterion; OR, odds ratio; CI, confidence interval; *MFD*, myofiber density; NS, not significant.)

**MFD* thresholds 546–551 indicate results with unadjusted *p*-values below 0.05 but above the Bonferroni-corrected significance threshold ($0.05/101 \approx 0.000495$).

Segmented Regression Analysis

In the segmented regression analysis for all parameters, the initial breakpoint visually estimated at 6 years of age (**Figure 11**). The slope of *MFD* exceptionally differed before and after this breakpoint, demonstrating a rapid decline in *MFD* up to approximately age 6 years with statistical significance (slope: -170.68 [CI -213.41 , -127.95]), after which the rate of decline markedly decelerated without statistical significance (slope: -28.31 [CI -76.47 , 19.85]) (**Figure 12**). The breakpoint itself was precisely estimated at 6.25 years [CI 5.08, 7.42] (**Figure 12**). This analysis yielded a high coefficient of determination (adjusted $R^2 = 0.80$). ANOVA comparing the simple linear regression model with the segmented regression model revealed a significantly improved model fit for the segmented regression ($F(2, 31) = 10.37, p < 0.001$). LOOCV yielded an RMSE of 151.44 compared to the original RMSE of 132.90 (ratio: 1.14), a mean breakpoint of 6.26 years (median: 6.25 years, range: 5.50 to 6.40 years), and an average CI ranging from 5.08 to 7.48 years.

On the other hand, other parameters demonstrated no statistical significance in the segmented modeling. Therefore, all subsequent statistical analyses were exceptionally applied to *MFD*.

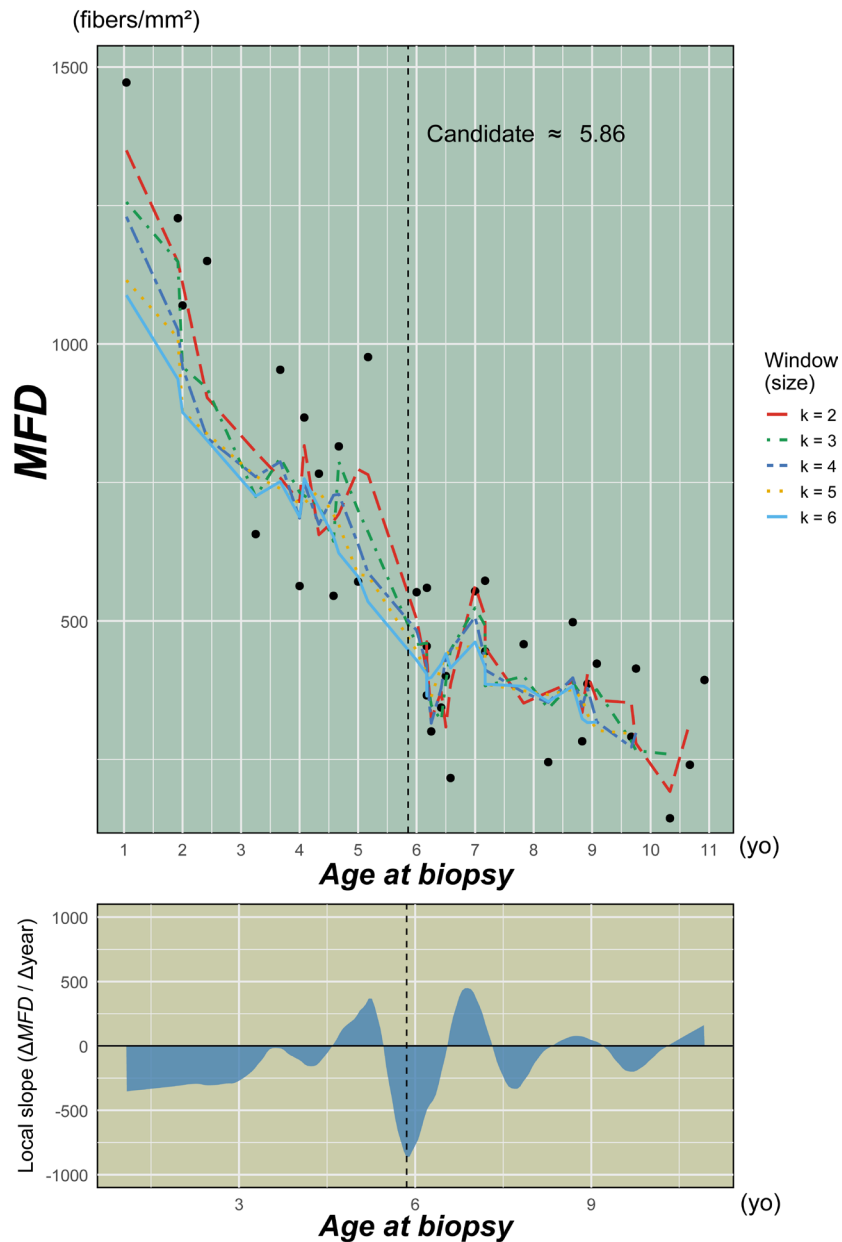


Figure 11: Mean-average plot of *MFD* in relation to *ABx*

The upper panel displays the moving-average curve (window size; $k = 2\text{--}6$) illustrating the relationship between *MFD* and *ABx*. The dashed vertical line indicates the steepest decline identified from the moving-average analysis, corresponding to a candidate breakpoint at 5.86 years. Individual data points represent actual patient measurements. The lower panel illustrates the local slope derived directly from the moving-average curve (window size; $k = 2$).

(**Abbreviations:** *MFD*, myofiber density; *ABx*, age at biopsy; RMSE, root mean squared error.)

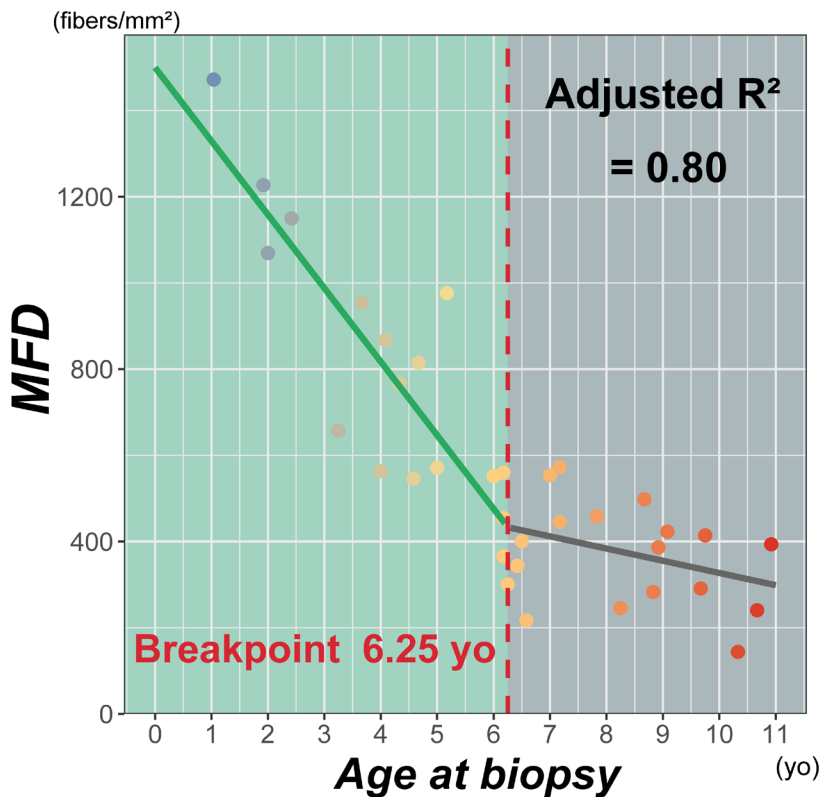


Figure 12: Segmented regression analysis

Segmented regression analysis demonstrates a statistically significant breakpoint at age 6.25 years (vertical dashed line). A rapid decline in *MFD* is evident before this age, with a subsequent plateauing of the rate of decline afterward.

(Abbreviation: *MFD*, myofiber density.)

MFD Replacement by ATPase-Stained Slide Samples

The values of *MFD* obtained via H&E-, G-T-, or M-T-stained slide samples were exploratorily replaced with those obtained from ATPase-stained slide samples (14 cases). This adjustment also resulted in near-complete separation between age groups before and after 6 years, except for a single case (subject 10) exhibiting a low *MFD* before age 6, with a strong Spearman's rank correlation coefficient for *ABx*-*MFD* ($\rho = -0.87$) across all 38 cases (Figure 13). Additionally, despite this replacement, *MFD* exhibited the same dynamics in the segmented regression analysis, characterized by a rapid decline before age 6 and stability thereafter. Notably, this adjustment identified a similar breakpoint age (6.42 [CI 5.28, 7.56]).

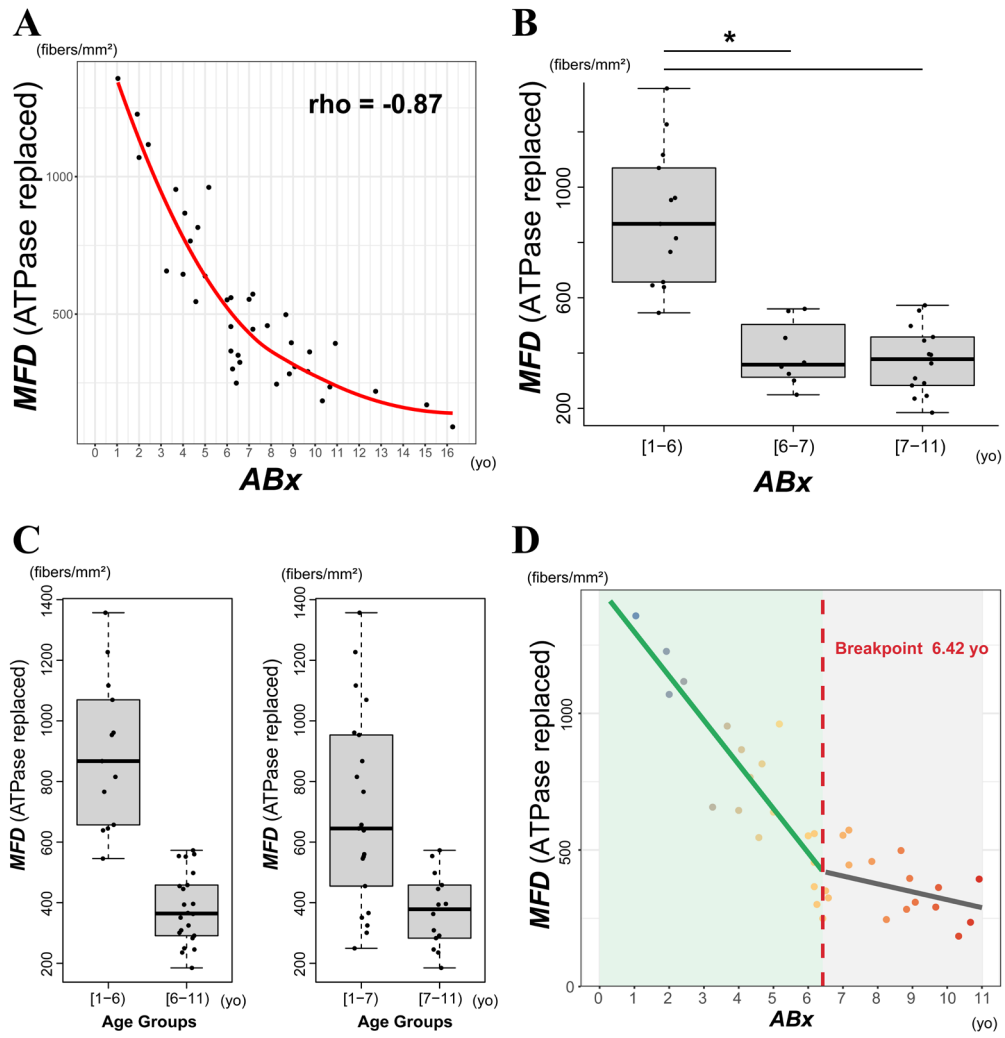


Figure 13: Replacement of MFD with ATPase-based measurements

- A:** Scatter plot demonstrates a strong inverse correlation between *ABx* and *MFD* after replacing original measurements with those derived from ATPase-stained samples.
- B:** Box plots illustrate ATPase-replaced *MFD* across the age stratification of 1–6, 6–7, and 7–11 years. Asterisk (*) denotes the statistical significances between age groups (for ages 1–6 vs. 6–7 years and 1–6 vs. 7–11 years).
- C:** Box plots comparing ATPase-replaced *MFD* using two different age-threshold cutoffs are shown: 1–6 vs. 6–11 years and 1–7 vs. 7–11 years. By presenting data in this comparative manner, this panel highlights age 6 as a critical histopathological threshold.
- D:** Segmented regression analysis demonstrates a statistically significant breakpoint at age 6.42 years (vertical dashed line).

(Abbreviations: ATPase, actomyosin adenosine triphosphatase; *ABx*, age at biopsy; *MFD*, myofiber density.)

Bayesian Analyses and Monte Carlo Simulations for MFD

First Bayesian segmented regression analysis indicated a posterior mean slope before the breakpoint (age 6.25) of -170.44 MFD/year [95% Credible Interval (CrI): $-207.47, -133.58$], and after the breakpoint, a posterior mean slope of -28.42 MFD/year [CrI: $-65.22, 8.77$]. Using a ROPE of $\pm 62.00\text{ MFD/year}$, derived from the difference between original and ATPase-replaced *MFD* values, no posterior estimates (0%) fell within this ROPE prior to the breakpoint, whereas nearly all posterior estimates (96.26%) fell within this ROPE after the breakpoint. Bayesian model comparison based on BIC yielded values of approximately 470.20 for the single-line regression model and approximately 455.82 for the segmented regression model, corresponding to an approximate BF_{10} of 1324. The sensitivity analysis using ROPE width defined as $+1SD$, $+1.5SD$, and $+2SD$ yielded posterior probabilities $>96\%$ (post-breakpoint) and $<0.5\%$ (pre-breakpoint), closely consistent with the aforementioned findings.

A Monte Carlo Method (2×10^6 replicates) quantified the probability that an *MFD*-based rule would place a muscle biopsy on the wrong side of the 6.25-year boundary; when the true age difference was 0.25 years ($\Delta MFD = 42.67$), the mean misclassification probability was 38.92%; this probability decreased monotonically to 1.21% when the age gap reached 2 years ($\Delta MFD = 341.36$), and the error rates for " $<6.25\text{ years}$ " and " $\geq 6.25\text{ years}$ " assignments remained symmetric throughout (Table 7).

Table 7: Monte Carlo simulation (2×10^6 replicates) of mean mis-classification

ΔABx	ΔMFD (fibers/mm ²)	Mis-classification <6 years	Mis-classification ≥ 6 years	Mean Error
0.25 years	42.67	38.96%	38.87%	38.92%
0.5 years	85.34	28.67%	28.65%	28.66%
0.75 years	128.01	19.93%	19.85%	19.89%
1 years	170.68	12.97%	13.01%	12.99%
1.25 years	213.35	7.93%	7.97%	7.95%
1.5 years	256.02	4.56%	4.56%	4.56%
1.75 years	298.69	2.43%	2.42%	2.43%
2 years	341.36	1.21%	1.22%	1.21%

(Abbreviations: *ABx*, age at biopsy; *MFD*, myofiber density.)

The second Bayesian posterior analysis of the *MFD* segmented regression model with weakly informative priors estimated a breakpoint at 6.37 years [CrI: 5.46, 7.40] (**Table 8**). Posterior slope estimates indicated a significant decline of -165.41 MFD/year [CrI: $-198.27, -133.88$] before the breakpoint and a substantially lower decline of -29.10 MFD/year [CrI: $-65.66, 11.90$] without statistical significance after the breakpoint (**Table 8**). Bayesian model comparison using LOOIC indicated that the segmented model had better predictive performance than a simpler linear model, with an expected log predictive density difference of 7.31. The posterior slope before the breakpoint was completely outside this ROPE interval. In contrast, the slope after the breakpoint overlapped the ROPE interval (95.01% of posterior distribution within ROPE; **Figure 14**).

Table 8: Bayesian segmented regression model with weakly informative priors*

Parameter	Mean	SD	2.5% CrI	Median	97.5% CrI
Intercept (pre-BP)	1459.61	81.67	1292.3	1460.28	1617.48
Slope (pre-BP) [†]	-165.14	17.34	-200.32	-164.87	-131.15
Slope (post-BP) [†]	-28.72	21.09	-67.84	-29.73	15.94
Breakpoint age (years)	6.37	0.58	5.24	6.37	7.66

(**Abbreviations:** BP, breakpoint; CrI, credible interval; ROPE, Region of Practical Equivalence; SD, standard deviation; ABx, age at biopsy; MFD, myofiber density.)

Weakly informative priors were set as follows (based on original segmented model): α (Intercept): normal(1500, 300); β_1 (Slope pre-breakpoint): normal($-171, 40$); β_Δ (Difference in slope): normal(142, 40); ψ^ (Breakpoint age; defined at zero on centered scale): normal(0, 2); error term (ε_i) $\sim N(0, \sigma^2)$.

[†] The fraction of posterior distribution within the ROPE was 0% for the pre-breakpoint slope, indicating robust statistical support for a non-zero slope before the breakpoint, and 95.01% for the post-breakpoint slope, showing practical equivalence to zero.

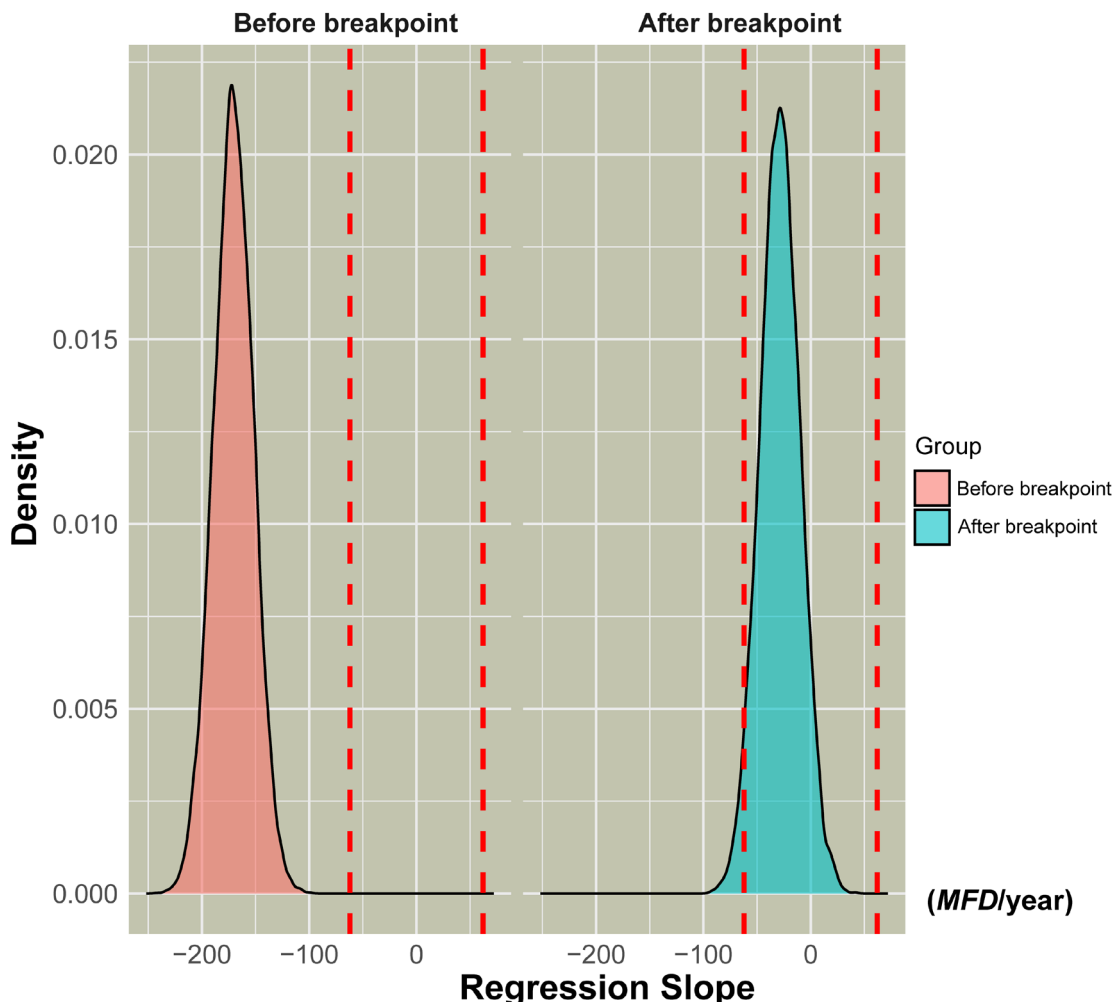


Figure 14: ROPE analysis

This plot presents the posterior distributions of the regression slopes obtained from the Bayesian segmented regression analysis, divided by the breakpoint. The left density plot (red) represents the posterior distribution of slopes after the breakpoint, while the right plot (blue) corresponds to slopes before the breakpoint. Dashed red lines indicate the ROPE ($\pm 62.00 \text{ MFD/year}$).

(**Abbreviations:** ROPE, Region of Practical Equivalence; *MFD*, myofiber density.)

The sample-size simulations using Monte Carlo method indicated that the sample size in the current study ($n = 35$) yielded 72.43% probability of detecting the breakpoint within ± 1.00 year, 79.47% within ± 1.25 years, and 84.54% within ± 1.5 years (**Table 9**).

Table 9: The results of sample-size simulations by Monte Carlo method*

Sample size	Precision (± 1 year) [†]	Precision (± 1.25 years) [†]	Precision (± 1.5 years) [†]
20	58.18%	65.43%	72.66%
25	65.65%	71.01%	76.77%
30	69.80%	76.43%	82.08%
35	72.43%	79.47%	84.54%
40	75.11%	81.64%	86.44%
45	77.00%	84.08%	88.16%
50	79.71%	86.14%	89.96%
55	81.59%	87.63%	91.58%
60	83.42%	89.01%	92.40%
65	84.51%	89.81%	93.87%
70	85.61%	90.65%	94.01%

* In each replicate, age at biopsy (ABx) values were bootstrapped from the observed <11 years cohort, while model parameters ($\beta_1, \beta_\Delta, \sigma, \psi$) were resampled from the Bayesian posterior ($n = 10,000$ draws). A run was counted as successful when the segmented-regression breakpoint lay within ± 1 , 1.25, and 1.5 years of the true ψ .

† Precision columns report the Monte-Carlo probability that the breakpoint estimate falls within ± 1.0 , 1.25, or 1.5 years of the posterior-sampled true breakpoint.

When the fitted logistic model established in the previous section was interrogated in terms of the conditional probability of being <6.25 years (rather than overall classification accuracy), three *MFD* cut-offs emerged. This regression analysis identified thresholds such that values ≥ 595.51 fibers/mm 2 corresponded to an approximately 80% probability of being younger than 6.25 years, values between 426.36 and 595.51 fibers/mm 2 defined a grey zone with approximately 50% probability, and values ≤ 426.36 fibers/mm 2 corresponded to an approximately 80% probability of being 6.25 years or older. Applying these cut-points allocated 10 cases to the high-probability " <6.25 years" zone, 11 to the grey zone and 14 to the low-probability " ≥ 6.25 years" zone ($ABx < 11$, $n = 35$; **Table 10**).

Table 10: Zone summary and *MFD* threshold

<i>MFD</i> zone	<i>MFD</i> threshold (fibers/mm ²)	Cases	Presumed therapeutic window*
High (≥80%, <6.25 years)	595.51	10	Large therapeutic window
Grey (20–80%, <6.25 years)	426.36–595.51	11	Requires individual judgement
Low (≥80%, ≥6.25 years)	426.36	14	Small therapeutic window

(Abbreviation: *MFD*, myofiber density.)

*Of note, the presumed therapeutic windows described here represent hypothetical classifications based solely on *MFD* thresholds derived from logistic regression probabilities; clinical validation of these categories was not performed in this analysis.

Revised Variance Analysis

Group-wise variance analysis showed significant pair-wise differences in *Mean*, *Sd*, and *Fat* between the Early band and each older band, a significant difference in *MFA* and in *Cov* only between Early and Late (**Figure 15**). In the Early–Late comparison, Cliff's δ indicated large effects for *Mean* ($\delta = 0.80$ [CI: 0.49, 1.00]), *Sd* ($\delta = 0.88$ [CI: 0.65, 1.00]), *Cov* ($\delta = 0.83$ [CI: 0.49, 1.00]) and *Fat* ($\delta = 0.75$ [CI: 0.36, 1.00]), while Hedges' d showed a pronounced decrease in *MFA* ($d = -1.36$ [CI: -2.54, -0.65]) and a large-magnitude increase in *CFA* ($d = 1.04$ [CI: 0.31, 2.16]); however, *CFA* did not attain statistical significance in the variance analysis. Full statistics, with *MFD* itself included as a positive control, are provided in **Table 11**.

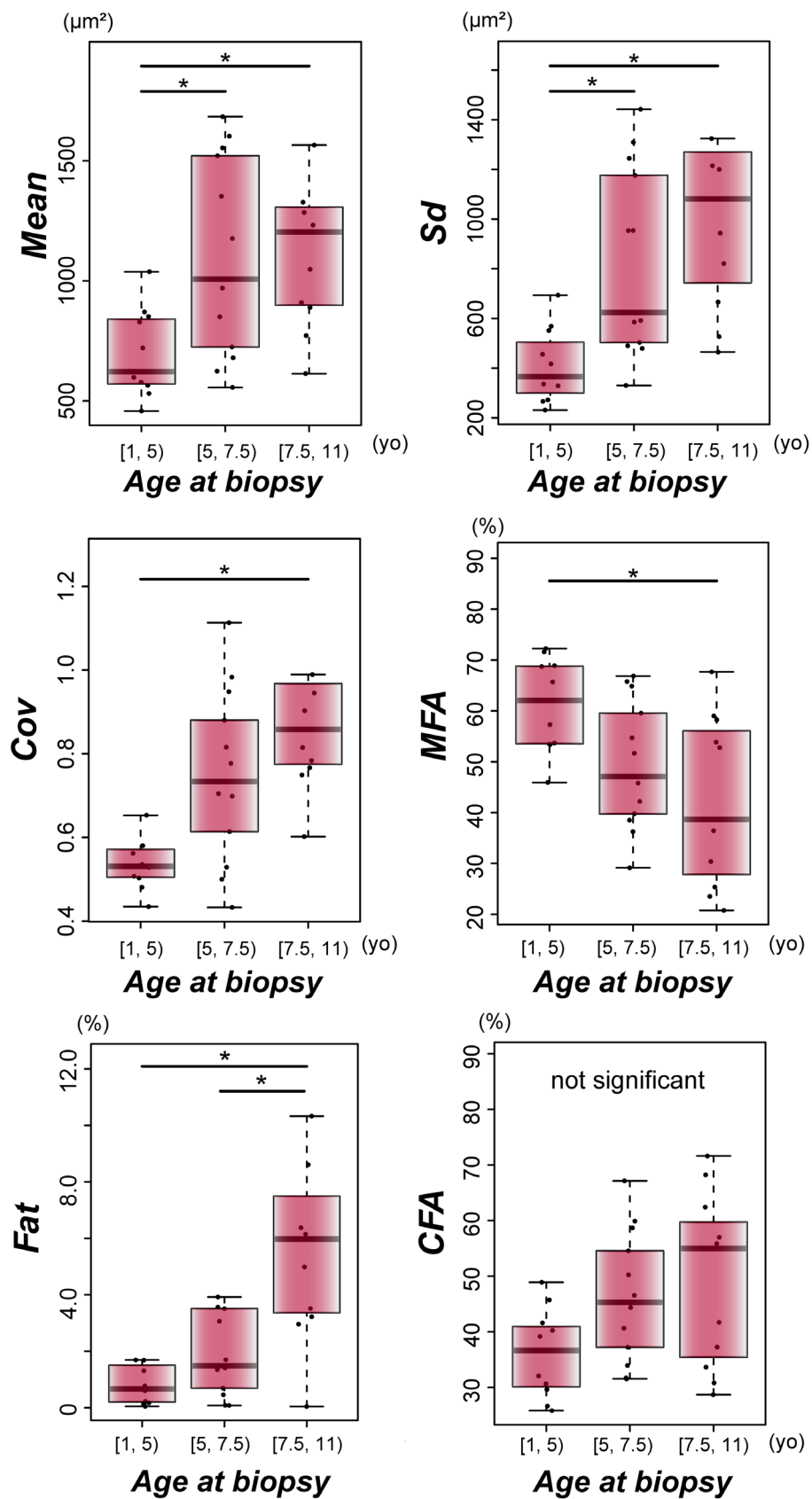


Figure 15: Box plots of revised variance analyses

Table 11: Revised variance analysis, effect size, and adjusted *p*-value with power

	Comparison	Effect size [95% CI]	Mean difference [95% CI]	<i>p</i> -value [‡]	Required [§]
Mean*	1–5 vs 5–7.5 years	0.61 [0.22 to 0.92]	403.72 [145.14 to 662.29]	<0.01	11.74
	1–5 vs 7.5–11 years	0.80 [0.49 to 1.00]	620.75 [93.48 to 1148.02]	<0.01	5.88
	5–7.5 vs 7.5–11 years	0.09 [−0.38 to 0.57]	217.03 [−345.70 to 779.77]	0.55	602.95
Sd*	1–5 vs 5–7.5 years	0.73 [0.38 to 0.97]	414.10 [180.25 to 647.95]	<0.01	7.43
	1–5 vs 7.5–11 years	0.88 [0.65 to 1.00]	861.90 [288.90 to 1434.90]	<0.0001	4.38
	5–7.5 vs 7.5–11 years	0.30 [−0.16 to 0.73]	447.80 [−154.31 to 1049.91]	0.18	53.58
Cov*	1–5 vs 5–7.5 years	0.48 [0.007 to 0.89]	0.16 [−0.019 to 0.33]	0.039	19.74
	1–5 vs 7.5–11 years	0.83 [0.49 to 1.00]	0.35 [0.12 to 0.59]	<0.001	5.24
	5–7.5 vs 7.5–11 years	0.40 [−0.06 to 0.79]	0.20 [−0.03 to 0.42]	0.064	29.75
MFD[†]	1–5 vs 5–7.5 years	−1.89 [−3.06 to −1.01]	−431.25 [−641.04 to −221.46]	<0.0001	6.35
	1–5 vs 7.5–11 years	−2.71 [−3.97 to −1.89]	−573.52 [−791.87 to −355.16]	<0.0001	3.75
	5–7.5 vs 7.5–11 years	−0.88 [−1.69 to −0.26]	−142.27 [−352.06 to 67.52]	0.23	21.43
MFA[†]	1–5 vs 5–7.5 years	−1.05 [−2.08 to −0.33]	−11.78 [−24.75 to 1.20]	0.12	15.39
	1–5 vs 7.5–11 years	−1.36 [−2.54 to −0.65]	−18.74 [−32.25 to −5.24]	0.015	9.52
	5–7.5 vs 7.5–11 years	−0.47 [−1.42 to 0.33]	−6.97 [−19.94 to 6.01]	0.4	72.31
Fat*	1–5 vs 5–7.5 years	0.36 [−0.10 to 0.78]	1.50 [−0.69 to 3.70]	0.15	37.6
	1–5 vs 7.5–11 years	0.75 [0.36 to 1.00]	5.28 [2.04 to 8.52]	<0.01	6.98
	5–7.5 vs 7.5–11 years	0.57 [0.12 to 0.94]	3.78 [0.12 to 7.44]	0.026	13.83
CFA[†]	1–5 vs 5–7.5 years	0.99 [0.31 to 1.92]	10.19 [−1.79 to 22.17]	0.16	16.89
	1–5 vs 7.5–11 years	1.04 [0.31 to 2.16]	13.19 [0.72 to 25.66] [¶]	0.11 [¶]	15.52
	5–7.5 vs 7.5–11 years	0.21 [−0.62 to 1.13]	3.00 [−8.98 to 14.98]	0.81	336.47

(Abbreviations: CI, confidence interval; *CFA*, connective/fibrotic tissue area; *Cov*, coefficient of variation of myofiber size; *Fat*, fatty degeneration area; *Mean*, mean myofiber size; *MFA*, myofiber area; *MFD*, myofiber density; *Sd*, standard deviation of myofiber size.)

* Cliff's δ for variables violating normality assumptions.

† Hedges' d for normally distributed variables with equal variances.

‡ False-discovery-rate-adjusted *p*-values

§ The per-group sample size required to detect the observed effect with 80% power.

¶ CI excludes zero, but adjusted *p* = 0.11 (>0.05); hence deemed not significant.

Discussion

Overview

The report by Peverelli et al. was considered extremely important for DMD muscle pathology research, and the present study was initially built upon their morphological observations, specifically highlighting the critical interval around ages 6–7 (Peverelli et al., 2015), which had been initially regarded with skepticism. This interval is marked by rapid and significant morphological changes in muscle tissues, as demonstrated by their analysis of 40 steroid-untreated samples. Their observations are now considered entirely reliable and their rationale, including insights into this critical interval, is supported by the findings presented here. However, while previous research predominantly used *MFA* along with connective tissue area or fibrotic changes as indices (Desguerre et al., 2009; Peverelli et al., 2015), this study has revealed that the number of muscle fibers per square millimeter provides a more dynamic and earlier indicator of pathological changes. This parameter is proposed as muscle fiber "density." Specifically, the current analysis reveals a rapid decline in *MFD* before the age of 6, challenging the previous understanding that muscular histological stability is maintained until the age of 6–7 years (Peverelli et al., 2015). These findings suggest a previously unrecognized subclinical phase of accelerated myofiber loss in the early stages of DMD.

Two key novel insights emerge from these analyses: (1) *MFD* serves as a sensitive surrogate biomarker for early-stage DMD progression, and (2) the identified age 6 threshold and the observed *MFD* dynamics delineate a critical histopathological transition in disease pathology. By capturing early tissue alterations undetectable by conventional indices, these results provide a potential framework for defining the optimal timing of corticosteroid initiation and other emerging therapies, thereby informing more individualized therapeutic decisions.

Morphometric Methodologies and Image Analyses

A distinguishing feature of this study is the use of archival muscle biopsy specimens collected over four decades ago. Although the primary analysis of this study focused on H&E-, G-T-, and M-T-stained slides, severely faded ATPase-stained specimens were also encountered, as exemplified by the specimen shown in **Figure 1A**, highlighting the extent of degradation observed. Although this specific ATPase-stained sample was not included in the quantitative analyses, the application of LUT-based digital restoration techniques underscores the feasibility of recovering highly

compromised histological materials at minimal cost. Notably, in an exploratory analysis, *MFD* values were substituted from 14 cases initially assessed via H&E/G-T/M-T staining with those derived from ATPase-stained slides. Despite this replacement, *MFD* exhibited the same dynamics, characterized by a rapid decline before age 6 and stability thereafter. Notably, this adjustment resulted in near-complete separation between age groups before and after 6 years, except for a single case (subject 10) exhibiting a low *MFD* before age 6, with a strong Spearman's rank correlation coefficient for *ABx-MFD* ($\rho = -0.87$) across all 38 cases (Figure 12), reinforcing both the robustness of *MFD* as a new metric and the efficacy of this color-restoration approach. Additionally, Focus Stacking was employed to mitigate focal plane variations attributable to uneven sectioning or mounting, facilitating the generation of high-resolution, well-focused images from suboptimal histological preparations. These methodologies hold broader implications for various pathology fields because they enable the partial revitalization of archival specimens compromised by diverse adverse conditions, thereby expanding opportunities for histopathological research and historical dataset utilization.

Given the scarcity of systematic histopathological studies in DMD, as described, the analyses of this study were partly guided by foundational insights previously reported by Peverelli et al. (Peverelli et al., 2015). Building on this, the morphological analysis in this study focused on the concept that ages 6–7 constitute a critical period in DMD progression, characterized by a significant increase in *CFA* accompanied by a decline in *MFA*, reflecting a loss of muscle self-regeneration and a transition toward fibrotic degeneration (Peverelli et al., 2015). Historically, MFS quantification in DMD histopathological research has often relied on semi-quantitative methods, while Bell and Conen employed the *Cov* to quantitatively evaluate MFS changes in 1967 under the technological constraints of that era (Bell and Conen, 1967; Desguerre et al., 2009; Peverelli et al., 2015).

In this study, because an objective and more precise assessment of MFS necessitates the enumeration of all individual myofibers, *MFD* values inherently emerged as part of the quantitative analytical framework. Notably, despite comparable *MFA*, a 1.5-fold difference in *MFD* was observed between patients aged 4 and 6 years (765.96 vs. 454.67; Figure 3A, 3B), underscoring a substantial histopathological distinction. Microscopically, densely packed myofibers may superficially convey an impression of increased *MFD*. However, the observations in this study suggest that mild hypertrophy may already be present before age 6, contributing to a uniform yet globally enlarged myofiber morphology that could obscure early-stage myofiber depletion upon

cursory examination. The stability of MFS-related parameters before age 6, particularly the narrow interquartile range of 0.50–0.56 in *Cov* (**Figure 10A, Table 3**), further supports this interpretation. Thus, these findings provide mechanistic insights into the differences in effect sizes observed between *MFA* and *MFD*.

Before the main statistical analysis, a thorough statistical evaluation using paired specimens stained with H&E and G-T methods was conducted, which demonstrated negligible batch effects and an exceptionally strong correlation between these two staining techniques. This approach, wherein correlation coefficients are employed as an alternative method to indirectly indicate that statistically significant differences are unlikely—since conventional statistical tests inherently cannot conclusively prove the absence of differences—is based on the exploratory approach described by Bell and Conen (Bell and Conen, 1967). The results of Bayesian analysis also confirmed the negligible batch effects between H&E and G-T methods. These findings strongly suggest that methodological variability arising from using multiple staining techniques did not significantly influence the results of the quantitative image analyses. Although comprehensive validation across all staining methods used in the present study would have been ideal, the rigorous comparative approach employed was considered sufficient to demonstrate methodological robustness and to validate the integration of data derived from multiple staining modalities. Future studies employing larger sample sizes under more rigorously controlled conditions are warranted to further substantiate the reliability and generalizability of the findings.

Exploratory Statistical Approaches

In statistical analysis, all parameters, including *ABx*, were treated as continuous variables. Initially, an age-predicting model was planned in order to establish an objective and reproducible method for evaluating muscular status in DMD, followed by correlation analysis for parameter selection. Subsequently, logarithmic transformation of the selected variables and multiple regression analysis with *ABx* as the dependent variable were performed. However, upon dividing the predicted values into more detailed age groups, it was found that prediction errors varied significantly across specific intervals. A Kruskal–Wallis test was then conducted to determine the age range within which prediction errors were minimized, revealing robust predictions up to approximately 7 years of age. Indeed, limiting the multiple regression to patients aged <7 years notably improved model fit, as indicated by a marked decrease in the AIC from 53.84 to 29.12. Furthermore, LOOCV confirmed that the restricted model (<7 years)

maintained comparable predictive accuracy (RMSE: 0.47) to the full-range model (RMSE: 0.49), supporting the robustness of the age-limited model. Verification for patients younger than 6 years was not feasible due to limited sample size. These findings suggest that histopathological evaluation using specific tissue markers is likely accurate up to approximately age 7, although further refinement within this critical interval is still required. It is not the diagnosis of DMD that becomes more difficult, but rather the evaluation of the disease progression in DMD patients. This observation implies that there is significant individual variability in the deterioration of muscle condition after the critical interval.

The approach used in this analysis—analyzing the difference between the actual and predicted *ABx* directly as a variable—is somewhat distinct from standard error analysis methods commonly applied in statistical contexts; typically, statistical error analysis aims to evaluate and improve prediction accuracy or model fit by assessing indices such as squared residuals, distribution of residuals, and metrics of model accuracy (e.g., residual standard error, R-squared statistic) (James et al., 2021). In contrast, the present study uniquely employs prediction errors themselves as data for further analysis, rather than simply assessing prediction accuracy. Specifically, the prediction errors (residuals) were used to investigate whether increased errors within certain age groups reflect underlying pathological changes. This approach involved performing variance analysis (Kruskal–Wallis test) on prediction errors across different age intervals. While non-standard from the perspective of conventional error analysis for predictive models, it appears that this approach remains scientifically valid. Analyzing residuals as data sources provided insight into appropriate age intervals for subsequent variance analysis, allowing the identification of distinct histopathological changes that would have been difficult to detect using traditional predictive modeling alone. Furthermore, without this residual analysis, defining precise age intervals would have been challenging, thereby limiting the ability to capture true variance in the subsequent analyses. This emphasizes the importance of exploratory analytic steps, even when they initially appear indirect or unconventional.

To further delineate age-dependent differences, variance analyses were conducted based on the pivotal age range identified by Peverelli et al. (Peverelli et al., 2015). By isolating the 6–7-year age group, it was found that *MFD* appeared nearly static within this interval, whereas others exhibited more pronounced changes, highlighting the significance of treating 6–7 years as a distinct period. Notably, these analyses demonstrated significant differences and large effect sizes in *MFD* between the

1–6 and 6–7 age groups, as well as between the 1–6 and 7–11 groups (**Table 3**). Additionally, a conventional histopathological parameter, *CFA*, exhibited significant differences between the same age groups, with large effect sizes, aligning with observations by Peverelli et al. Although individual-level data are unavailable, approximate estimates derived from their summary data (Peverelli et al., 2015) suggest a large effect size (e.g., Cohen's *d*: 1.96 [CI 1.19, 2.73]). In addition, while large effect sizes were detected in variance analysis comparing age groups (1–6 vs. 6–7 and 7–11 years), the actual data revealed considerable overlap among these age groups, with some patients older than age 6 showing *CFA* values similar to those younger than age 6. Furthermore, although the variance analysis results reported in the main text indicated a significant difference in *CFA* between the 1–6 year and 7–11 year age groups, a subsequent review applying a false-discovery-rate correction showed that the difference was not statistically significant (*p* = 0.055). This suggests that individual variability in *CFA* tends to widen with increasing age, a factor potentially responsible for large effect sizes observed in group-level analyses. Such variability might explain the discrepancies and differing interpretations among previous studies (Cardone et al., 2023; Desguerre et al., 2009; Peverelli et al., 2015). Considerable inter-individual variability in *CFA* is indicated in the present study, and this variability is regarded as the principal reason for the discrepancy with the findings of Peverelli et al., who obtained statistical significance by calculating *CFA* through multi-stage averaging during their statistical analysis (Peverelli et al., 2015). Accordingly, the present findings support the report by Cardone et al., which detected no correlation between *CFA* and age (Cardone et al., 2023). Additionally, it is proposed that evaluating *Opaque* and *IntN* as a proportion relative to *MFD* provides a more accurate assessment than counting absolute numbers per FOI, since the pathological significance of these fibers likely varies depending on overall *MFD*. For instance, identifying 10 abnormal myofibers in an FOI with an *MFD* of 1000 should be interpreted differently from observing the same number in an FOI with an *MFD* of 300. Moreover, inconsistent findings across studies (Cardone et al., 2023; Desguerre et al., 2009; Peverelli et al., 2015) suggest limited specificity and reproducibility of these histological parameters. Thus, previous reports including this study suggest that these conventional histopathological parameters may have inherent limitations, suggesting they might not serve as reliable markers for accurately tracking disease progression of DMD.

Although the specific numerical thresholds identified through logistic regression (approximately 560–563 fibers/mm², **Table 6**) may be dataset-specific due to

the exploratory nature of the analysis in this study, they clearly underscore age 6 as a critical juncture in disease progression. The number of events in the present logistic regression model was 13, satisfying the commonly recommended criterion of at least 10 events per explanatory variable (Peduzzi et al., 1996), thereby mitigating concerns about potential overfitting. However, logistic regression alone could not definitively confirm whether this threshold truly represented the critical age of disease transition or merely reflected the chosen reference age in the logistic model.

To address this limitation, segmented regression analysis was implemented, as described above, which provided objective statistical confirmation of the critical breakpoint at approximately 6.25 years, clearly revealing distinct regression slopes before and after this point. Nevertheless, given the inherent nature of the statistical approaches, it should be acknowledged that the exact numerical threshold identified may be dataset-specific. Therefore, in practical terms, it may be more appropriate to interpret the breakpoint's CI ([5.08, 7.42] and [5.28, 7.56]) as representing either a critical age period (around ages 5 to 7.5 years) or an alternative transitional phase rather than a definitive single age cutoff.

Bayesian methods further reinforced the reliability of segmented regression results, demonstrating clear difference between the rates of *MFD* decline before and after this age threshold. To validate the results of segmented regression analysis, frequentist methods had inherent limitations. Although bootstrap methods might initially appear suitable, the characteristics inherent to segmented regression analysis necessitate different considerations. Since the primary analysis involves evaluating differences in *MFD* dynamics before and after a breakpoint, randomly resampled datasets generated by bootstrapping must contain a sufficient number of data points both before and after this breakpoint; otherwise, the bootstrap results become unstable. To the author's knowledge, there is no existing literature specifically addressing how to validate segmented regression results using frequentist approaches. However, analogous guidance exists for logistic regression analysis, which recommends a minimum of 10 events to ensure reliability (Peduzzi et al., 1996). It seems reasonable to adopt a similar principle for segmented regression. Yet, implementing a bootstrap procedure with such strict minimum data requirements in R would likely result in frequent errors and unstable analyses. Furthermore, restricting resampling in a bootstrap to maintain sufficient data points contradicts the fundamental assumption of random sampling with replacement, introducing methodological inconsistencies. Overcoming these methodological barriers thus emerged as a significant challenge in segmented regression

analysis. This concern is discussed again later.

Therefore, Bayesian statistical approaches employing probability distributions were deemed more suitable for validation in this context. Monte Carlo-based approaches, of which bootstrapping itself is a form, are more effectively integrated within a Bayesian framework. In this study, two Bayesian methods were employed: one using conjugate posterior distributions with a fixed breakpoint at 6.25 years, and another incorporating weakly informative priors based on the results from segmented regression analysis. The former approach provides convenient results without requiring Markov Chain Monte Carlo simulation but cannot estimate the breakpoint itself. This method primarily validates the estimated slopes before and after the breakpoint and assesses the improvement of the segmented regression model over a simple linear regression. Additionally, logistic regression analyses using an 80% cutoff for *MFD* values and Monte Carlo simulations estimating misclassification rates across age intervals were conducted. Although these results are summarized earlier, whether these analyses are sufficiently rigorous depends on how extensively sensitivity analyses of segmented regression should be pursued. Given the inherent limitation that external validation was not feasible, it was concluded that a more rigorous Bayesian approach capable of estimating breakpoints was also necessary. This approach carries substantially higher computational costs and greater difficulty in setting appropriately weakly informative priors.

Regarding weakly informative priors, the SDs for slopes before and after the breakpoint were set based on doubled standard errors obtained from segmented regression analysis. Additionally, the SD for the breakpoint prior was set at 2 (approximately the width of the 95% CI of the estimated breakpoint), sufficiently capturing uncertainty. Finally, the SD for the intercept prior was taken directly as the observed SD of the *MFD* values. Bayesian analysis results clearly supported the segmented regression findings, including breakpoint estimation. Furthermore, to validate the adequacy of the sample size and enhance the robustness of the present findings, a frequentist Monte Carlo simulation approach was also employed. This approach was chosen because it effectively addresses the inherent limitations of the bootstrap method—specifically, the frequent occurrence of severely unbalanced samples around the breakpoint as described—by repeatedly generating synthetic datasets and assessing the proportion of successful estimations. In addition, given that the core analytical approach was segmented regression rather than variance analysis (including effect size calculations), verifying sample size adequacy specifically for segmented

regression was essential.

Ultimately, Monte Carlo methods played a crucial role in both frequentist and Bayesian analyses within this study. Although various validation methods were used here, these methods will be particularly useful in future analyses involving external datasets or animal studies. Given the inherent limitations of this retrospective observational study, external validation is essential moving forward. The analytical techniques, statistical scripts, and simulation methods developed here will likely serve as valuable tools in future investigations requiring *MFD* dynamics or critical threshold analyses. For example, ongoing research plans include identifying critical age (e.g., months old) using *MFD* analysis in *mdx* mouse models and conducting multi-omics analysis around identified critical age to pinpoint specific molecular targets. The image analysis methods, statistical techniques, analytical scripts, and sample-size simulation results established in this study will undoubtedly play important roles in future research on DMD.

Suggested Histopathological Inflection Point

It is proposed that age 6 represents a histopathological inflection point in the progression of DMD, coinciding with a peak in early muscle deterioration as indicated by a marked reduction in *MFD*. Beyond this age, disease progression appears to transition into a more heterogeneous phase, potentially reflecting inter-individual variability in pathological remodeling, which may explain the marked dispersion observed in other conventional parameters such as *MFA* and *CFA*. While it has been posited that the pathophysiology of DMD is driven by recurrent cycles of necrosis and regeneration, ultimately culminating in an incomplete compensatory process (Nonaka and Nishino, 2021), the findings observed in this study indicate that a substantial decline in *MFD* is already evident between ages 1 and 6, followed by stabilization at lower values. This observation suggests that inadequate muscle regeneration begins in the early stages of DMD and subsequently contributes to progressive tissue remodeling. Moreover, these findings indicate that while reductions in *MFA* and increases in connective tissue become more pronounced after age 6–7, these histopathological transitions remain consistent with previous observations (Peverelli et al., 2015).

The author firmly believes that the abrupt morphological changes observed in the muscles of DMD patients around the ages of 6–7 years are undeniable. As described, this study has demonstrated that the *MFD* in DMD patients continues to decline rapidly before the age of 6 years. There appears to be a physiological threshold

for *MFD*. Until this threshold is reached, significant morphological changes in the muscles are not evident. However, once the *MFD* falls below the threshold, muscle homeostasis would be disrupted, leading to rapid and "easily noticeable" morphological changes. This study may imply the existence of such a physiological threshold in *MFD*, which is critical for understanding the progression of DMD. Of course, it should also be noted that some patients exhibited *MFD* values above the threshold even after the age of 6, or below the threshold even before the age of 6, indicating that there are a certain range of *MFD* threshold which could be altered by not only individual differences but also various circumstances of research, other datasets, sample size, or sample condition.

Clinical Relevance

Clinical manifestations of DMD, including difficulties with stair climbing, waddling gait, and frequent falls, typically emerge between the ages 3 and 5 years (Birnkraut et al., 2018b; Crisafulli et al., 2020; van Dommelen et al., 2024). Additionally, contractures of the iliotibial bands, hip flexors, and heel cords become apparent before the age of 6 years (Brooke et al., 1983). Notably, Zatz et al. reported that serum CK levels in DMD patients are already elevated within the first year of life, progressively increasing until approximately age 6, after which they decline as a result of progressive muscle degeneration (Peverelli et al., 2015; Zatz et al., 1991). Moreover, McDonald et al. reported a marked decline in performance on the 6-minute walk test around age 7 years in DMD patients (McDonald et al., 2013), similarly highlighting a critical functional downturn around ages 6–7 years. Mayhew et al. also demonstrated that steroid-naïve DMD boys aged 7 years exhibit significantly lower velocities in rise-from-floor and 10-meter walk/run tests compared to those aged 4–6 years, further reinforcing the functional downturn observed around this age range (Mayhew et al., 2022). The observed histopathological findings in this study coincide with these clinical observations; however, further validation is necessary due to the retrospective and exploratory nature of the analysis in this study.

MFD dynamics may also offer a mechanistic explanation, at least partially, for calf muscle pseudohypertrophy. While pseudohypertrophy has traditionally been attributed to fat and connective tissue infiltration (Walters, 2017), *MFD* dynamics indicate that the subtle yet homogeneous myofiber hypertrophy observed between ages 1 and 6, in conjunction with stable Cov, supports prior evidence suggesting that true myofiber hypertrophy contributes to calf enlargement in the early stages of DMD (Nonaka and Nishino, 2021; Walters, 2017).

The observations in this study have important insights into therapeutic strategies. A clustering-based analysis by Fang et al. demonstrated that DMD patients who received higher cumulative steroid exposure before age 6 exhibited slower disease progression compared with those who initiated corticosteroid therapy after this age, highlighting a critical therapeutic window (Fang et al., 2023). McDonald et al. reported that, among patients aged ≥ 7 years, ambulatory function progressively declined over 48 weeks regardless of steroid treatment status (McDonald et al., 2013). Importantly, they suggest that certain therapeutic agents, such as exon-skipping therapies aimed at restoring dystrophin expression, likely require a sufficient proportion of viable myofibers for optimal efficacy, providing suggestive insights that align with the observed *MFD* dynamics (McDonald et al., 2013). While multiple clinical guidelines recommend early corticosteroid initiation depending on specific clinical conditions such as early functional decline, the optimal timing remains uncertain because of the absence of robust foundational evidence (Birnkrant et al., 2018b; Duan et al., 2021; Fontaine Carbonnel et al., 2024; Matthews et al., 2016). Furthermore, concerns regarding potential adverse effects, including growth suppression, impaired growth inhibition, bone metabolism, and excessive weight gain, are well-documented (Birnkrant et al., 2018b). Recent randomized controlled trials investigating vamorolone—a dissociative steroid anti-inflammatory agent—demonstrated that treatment of steroid-naïve DMD patients aged 4–7 years yielded motor outcomes comparable to those of prednisone while mitigating detrimental effects on growth and bone health (Dang et al., 2024; Guglieri et al., 2022), thus supporting the feasibility of earlier therapeutic intervention.

Implications for Disease Progression Assessment

This clinical scenario underscores the growing need for reliable biomarkers that can objectively inform the timing and appropriateness of early therapeutic initiation. In this context, *MFD* could serve as an objective, pathology-based biomarker, facilitating more individualized and evidence-based clinical decision-making. For clinical application, it would be desirable to establish baseline *MFD* thresholds in DMD disease course through future natural history studies. However, given the increasing emphasis on earlier corticosteroid and steroid-sparing interventions (Dang et al., 2024; Fang et al., 2023; Guglieri et al., 2022), the recruitment of completely steroid-naïve DMD cohorts for natural history studies will become increasingly challenging from an ethical standpoint. Nonetheless, large-scale validation studies—including both steroid-treated and untreated cohorts—are imperative to further substantiate these findings. Moreover,

it remains unclear whether the low and stable *MFD* dynamics observed after age 6 represent an irreversible state or if these dynamics could potentially be reversed by effective therapeutic interventions, as the observations in this study are based solely on steroid-naïve patients. On the other hand, muscle biopsy remains an important tool in contemporary clinical trials, serving as both a primary and secondary outcome measure in the evaluation of novel therapeutic strategies (Boehler et al., 2023; Frank et al., 2020; Mendell et al., 2020, 2013). Therefore, for clinical trials already employing muscle biopsy as an endpoint, it is recommended to incorporate longitudinal assessment of *MFD* dynamics as a monitoring tool alongside conventional motor and/or functional evaluations. Counting-based *MFD* assessment is highly feasible, and currently available digital tools (Dubuisson et al., 2022) capable of automating myofiber enumeration can further facilitate routine clinical implementation.

A noninvasive method to evaluate *MFD* would be highly desirable. Although magnetic resonance imaging can detect relatively pronounced pathological changes such as fat replacement or connective tissue increase (Finanger et al., 2012; Hollingsworth et al., 2013), its sensitivity to subtle histological alterations at the myofiber level is uncertain. In addition, the results of the statistical analyses also highlight the limitations of current radiologic imaging analyses in DMD research. While they are noninvasive and beneficial for repeated assessments (Finanger et al., 2012; Hollingsworth et al., 2013; Mathur et al., 2010), they have not yielded significant breakthroughs in understanding muscle pathology.

In this study, parameters quantified by "area" measurement did not seem to contribute effectively to evaluating disease progression. Furthermore, the lack of specificity in traditional imaging analyses of *MFA*, necrotic tissue, fat, and connective tissue changes underscores the need for more effective approaches such as radiomics and deep learning (Moreno et al., 2021; Pinheiro et al., 2020; Rinaldi et al., 2023; Shiri et al., 2022). Recently, CT-based radiomics has shown potential in detecting histologically subtle features in oncology imaging, such as lung cancer invasiveness, lymphovascular invasion, and other prognostically relevant histopathological features (Cheng et al., 2024; Jiang et al., 2020). Its utility in quantifying early myofiber alterations in DMD remains unexplored but warrants investigation, awaiting future radiological-histological correlation studies.

Clinical-Statistical Integration for Practice

The segmented regression model produced a RMSE of 132.90, indicating that

observed *MFD* values deviate from the fitted line by, on average, about ± 133 fibers/mm 2 . Treating this figure as the empirical standard deviation of vertical error, a horizontal age shift (ΔABx) can be translated into an expected vertical shift on the steep, pre-breakpoint limb via [$\Delta MFD = |\text{slope}| \times \Delta ABx$].

Monte Carlo experiments used this link to ask how often a single muscle biopsy in DMD patient would be placed on the wrong side of the 6.25-year threshold. With two million replicates per scenario, mis-classification remained high (approximately 39%) when the true ages differed by only ± 0.25 years but fell briskly as the gap widened. At a separation of ± 1 year the mean error fell below 13%, and at ± 1.25 years it reached below 8%, corresponding to approximately 92% correct discrimination between children younger than 6.25 years and those 6.25 years or older. Notably, false-positive and false-negative rates were symmetric across the entire range, indicating that the rule is directionally unbiased.

Because clinical decisions are rarely binary, the logistic model established in this study was also interrogated for the conditional probability of being <6.25 years at any given *MFD* value. The 20% and 80% posterior probabilities mapped to cut-points of 426.36 and 595.51 fibers/mm 2 , respectively. These translate into three practical zones: a high-probability zone (≥ 595.51 fibers/mm 2) in which $\geq 80\%$ of cases are likely <6.25 years and the therapeutic window may be large; a grey zone (426.36–595.51 fibers/mm 2) where probability hovers around chance and individual clinical judgement is required; and a low-probability zone (≤ 426.36 fibers/mm 2) where $\geq 80\%$ of biopsies come from patients ≥ 6 years and the therapeutic window may be small.

Taken together, the analysis indicates that the simple age cut-off is highly reliable for patients younger than 5 years or older than 7.5 years of age. Within roughly the ± 1.00 -year band around the 6.25-year breakpoint, however, clinicians should rely less on a strict dichotomy and more on the *MFD* probabilistic zones—integrated with the broader clinical picture—to guide therapy. Importantly, the optimal way to weight these *MFD* probability bands against individual clinical factors remains uncertain and should be clarified by future clinicopathological research.

Study Limitations

This study had several limitations. First, when validating the variability of preparation and staining methods, ideally, rigorous validation would have included all staining methods used (H&E, G-T, M-T) and direct comparisons between frozen and FFPE samples. However, due to limitations in sample availability, comprehensive

evaluation beyond the H&E and G-T comparison was not feasible.

Second, in statistical analysis, the small sample size may have contributed to wider CIs for the estimated effect sizes, potentially reducing statistical power and increasing the uncertainty of the results. Moreover, although the present logistic regression model satisfied the recommended 10 events-per-variable criterion (Peduzzi et al., 1996), this modeling was exploratory in nature. Furthermore, a larger sample would allow more granular age stratification, which could facilitate the identification of subtler, age-specific histopathological changes.

Third, regarding the study design, despite the single-center retrospective analysis ensured standardized clinical protocols, biopsy sites (quadriceps femoris), and slide preparation methods, it inherently introduces selection biases and limits the generalizability of findings to broader populations.

Fourth, the availability of clinical data was substantially limited due to the historical nature of the archived biopsy specimens. Specifically, detailed longitudinal clinical data, such as motor/physical function assessments, precise symptom onset timing, and genetic characterization for all patients, were unavailable for the majority of cases. Consequently, comprehensive clinicopathological correlations could not be performed. Future prospective studies incorporating robust clinical datasets are needed to elucidate the clinical relevance of histopathological findings observed at early stages of DMD.

Fifth, this study relied on archival biopsy samples preserved over four decades, potentially introducing batch effects due to variations in storage duration and subtle differences in tissue preservation conditions. Although preliminary analyses demonstrated statistical comparability between staining methods (H&E and G-T), the possibility of unrecognized variability or residual effects related to long-term preservation cannot be completely ruled out.

Finally, although *MFD* is a straightforward measure with high reproducibility and practicality, it inherently simplifies complex histopathological processes in muscle into a single numerical index, potentially limiting comprehensive pathophysiological interpretation. In the present study, sample size constraints limited statistical analyses primarily to univariate or simple multivariate models (e.g., multiple regression using *MFD* and *Sd*). A larger sample size would have enabled more robust multivariate analyses, potentially revealing additional subtle or interactive pathological factors and enhancing the current understanding of early-stage DMD progression.

Therefore, a longitudinal, multicenter study design involving both steroid-

untreated and steroid-treated cohorts and incorporating multivariate statistical modeling could provide deeper insights into how these early muscle tissue alterations influence disease progression over time.

Issues of This Study and Perspectives for Future Research

Despite the inherent constraints associated with archival specimens, the methodological approaches utilized in this study provided a novel perspective on early-stage DMD and its clinical significance.

Reflecting on the intrinsic challenges encountered in this study is essential. It is clear that this research inherently possesses a different kind of difficulty compared to other studies, arising not solely from methodological or analytical complexity but more fundamentally from differences in "evaluation criteria" and "field-specific expectations." For instance, in cancer pathology and oncology research, molecular biology approaches such as genetic analysis and targeted therapies are well-established and clearly recognized evaluation standards. Studies integrating morphological and immunohistochemical assessments with molecular pathological analyses using advanced techniques, such as comprehensive genomic profiling, therefore benefit from readily accepted objective validity and well-defined interpretative guidelines, no matter how complex the methods involved may be. In contrast, studies such as the present one, which rely predominantly on quantitative morphometric analyses of archival specimens without the support of predefined analytical frameworks, inherently face unique challenges in gaining immediate recognition and validation within the scientific community.

In the author's prior experience, even single-case studies can achieve international scientific adoption if they clearly align with established evaluation frameworks. There are two research projects independently initiated and completed during the doctoral course (in these studies, the LUT-adjustment technique and Focus Stacking were used). Last year, the author reported the first case of morular metaplasia within a high-grade sporadic gastric foveolar-type adenoma (Yamakado et al., 2024). Although this metaplasia had never been previously documented in gastric tumors, the existence of well-established immunohistochemical evaluation criteria in other organs allowed for the credibility and scientific adoption of this rare entity, even in a single-case observation. Similarly, in a separate study, the author described a case of pulmonary adenocarcinoma that spontaneously transformed into large cell neuroendocrine carcinoma with *MYC* amplification (Yamakado et al., 2025). Despite the

limitation that such a phenomenon inherently requires continuous observation for morphological confirmation, detailed morphological analysis and comprehensive next-generation sequencing demonstrated objective validity owing to well-documented genome analytical evaluation criteria, strengthening scientific credibility. Thus, these two surgical-pathology papers stand as precedents that demonstrate technical proficiency in tackling rare cases, yet they derived their evaluative metrics from pre-existing external frameworks. However, the present study was burdened by the necessity of stepping outside established analytical frameworks, consequently lacking well-defined evaluation criteria or established methodological precedents, resulting in inherent difficulties regarding scientific validation and adoption. Although all three papers were produced during the doctoral course, their character differs markedly.

From a translational research standpoint as well, the present study encountered several challenges. As described, throughout the project, the following steps had to be undertaken: establishment of methods for data generation, development of quantitative assessment methodologies, selection of appropriate statistical analyses, and formulation of interpretation criteria for the obtained results. However, such an approach can easily appear more subjective, requiring rigorous justification against potential criticism, such as "Why should clinically significant interpretations be derived from such simple counting data?" Thus, this approach relies heavily on the researcher's effort for logical interpretation and persuasive argumentation to establish the scientific validity and significance of the findings. Furthermore, in the context of a chronic progressive disorder such as DMD, demonstrating clinical relevance necessitates evidence of subtle changes and thresholds associated with disease progression. Frequently, studies such as this research do not directly result in clear therapeutic pathways or immediate clinical decision-making. Consequently, it becomes particularly challenging to persuasively develop arguments connecting these subtle pathological findings to meaningful clinical implications or therapeutic strategies. Accordingly, it can be concluded that the challenges pointed out thus far have not been fully resolved within the present study, and that subsequent investigations—coupled with external validation and clinical exploration—will be required to establish an objective evaluation framework and secure robust generalizability.

In summary, the intrinsic challenges of this research arose primarily from the necessity of developing entirely new evaluation criteria rather than relying on established analytical methods or validated biomarkers. Overcoming these challenges led to the identification of the critical age threshold around 6 years and the characteristic

pattern of *MFD* decline, which may represent key benchmarks for assessing disease progression, potentially informing clinical practice. Of course, validation through larger, controlled studies remains essential. The author believes that the findings of this study support the broader utilization of archival samples and contribute to the advancement of future translational research, thereby refining the understanding of DMD's natural history and enhancing therapeutic decision-making for this severe devastating disease.

Conclusions

Significant Insights from This Study

1. *MFD* (myofiber density) serves as a sensitive surrogate biomarker for early-stage DMD progression, suggesting a previously unrecognized subclinical phase characterized by accelerated myofiber loss.
2. The identified age around 6 years threshold and the observed *MFD* dynamics delineate a critical histopathological transition in disease progression, thereby providing deeper insights into the natural history of DMD.
3. The original semi-quantitative image analysis approach, incorporating novel digital restoration techniques (such as LUTs adjustment and Focus Stacking), effectively captures early subtle tissue alterations, providing a potential framework to inform and enhance clinical decision-making.

Directions of Future Research on DMD Pathology

1. Longitudinal and multicenter studies that systematically investigate the influence of early histopathological alterations (e.g., *MFD* dynamics) on long-term disease progression, functional outcomes, and therapeutic responsiveness are needed.
2. Expanded patient cohorts, encompassing both steroid-treated and steroid-naïve individuals, are essential to validate the robustness and clinical utility of *MFD* as a biomarker, as well as to clarify potential steroid-induced histopathological changes.
3. It is anticipated that broader utilization of archival specimens in translational research will be encouraged, leveraging novel restoration methods such as LUT-based digital enhancement and Focus Stacking to expand retrospective analyses, refine historical benchmarks, and inform future clinical guidelines.

Potential Issues

1. Recruitment barriers for steroid-naïve patients should be considered. As therapeutic strategies increasingly emphasize early corticosteroid initiation or steroid-sparing alternatives, ethical constraints will complicate the enrollment of untreated cohorts, thereby restricting natural history studies.
2. The reversibility of *MFD* alterations is uncertain. It remains critical to elucidate whether the low, stabilized *MFD* observed after the identified threshold (age 6) reflects a definitive, irreversible shift in muscle pathology or if these changes may be responsive to therapeutic interventions.

Acknowledgement

The author would like to acknowledge Editage's (www.editage.com) support in manuscript editing. The author is also deeply grateful to Dr. Zen-ichi Tanei and Prof. Shinya Tanaka (Department of Cancer Pathology, Graduate School of Medicine, Hokkaido University, Sapporo, Hokkaido, Japan) for their dedicated guidance and continuous support. The author furthermore wishes to express sincere gratitude to Dr. Yusuke Ishida (Department of Pathology, National Hospital Organization Hokkaido Medical Center, Sapporo, Hokkaido, Japan) for his invaluable advice.

Conflicts of Interest

The author declares no conflicts of interest. No funds were received for this study.

References

- Bell, C.D., Conen, P.E., 1967. Change in fiber size in Duchenne muscular dystrophy. *Neurology* 17, 902–13.
- Bez Batti Angulski, A., Hosny, N., Cohen, H., Martin, A.A., Hahn, D., Bauer, J., Metzger, J.M., 2023. Duchenne muscular dystrophy: disease mechanism and therapeutic strategies. *Front Physiol* 14, 1183101.
- Biggar, W.D., Skalsky, A., McDonald, C.M., 2022. Comparing Deflazacort and Prednisone in Duchenne Muscular Dystrophy. *J Neuromuscul Dis* 9, 463–476.
- Birnkrant, D.J., Bushby, K., Bann, C.M., Alman, B.A., Apkon, S.D., Blackwell, A., Case, L.E., Cripe, L., Hadjiyannakis, S., Olson, A.K., Sheehan, D.W., Bolen, J., Weber, D.R., Ward, L.M., DMD Care Considerations Working Group, 2018a. Diagnosis and management of Duchenne muscular dystrophy, part 2: respiratory, cardiac, bone health, and orthopaedic management. *Lancet Neurol* 17, 347–361.
- Birnkrant, D.J., Bushby, K., Bann, C.M., Apkon, S.D., Blackwell, A., Brumbaugh, D., Case, L.E., Clemens, P.R., Hadjiyannakis, S., Pandya, S., Street, N., Tomezsko, J., Wagner, K.R., Ward, L.M., Weber, D.R., DMD Care Considerations Working Group, 2018b. Diagnosis and management of Duchenne muscular dystrophy, part 1: diagnosis, and neuromuscular, rehabilitation, endocrine, and gastrointestinal and nutritional management. *Lancet Neurol* 17, 251–267.
- Birnkrant, D.J., Bushby, K., Bann, C.M., Apkon, S.D., Blackwell, A., Colvin, M.K., Cripe, L., Herron, A.R., Kennedy, A., Kinnett, K., Naprawa, J., Noritz, G., Poysky, J., Street, N., Trout, C.J., Weber, D.R., Ward, L.M., DMD Care Considerations Working Group, 2018c. Diagnosis and management of Duchenne muscular dystrophy, part 3: primary care, emergency management, psychosocial care, and transitions of care across the lifespan. *Lancet Neurol* 17, 445–455.
- Boehler, J.F., Brown, K.J., Beatka, M., Gonzalez, J.P., Donisa Dreghici, R., Soustek-Kramer, M., McGonigle, S., Ganot, A., Palmer, T., Lowie, C., Chamberlain, J.S., Lawlor, M.W., Morris, C.A., 2023. Clinical potential of microdystrophin as a surrogate endpoint. *Neuromuscul Disord* 33, 40–49.
- Brooke, M.H., Fenichel, G.M., Griggs, R.C., Mendell, J.R., Moxley, R., Miller, J.P., Province, M.A., 1983. Clinical investigation in Duchenne dystrophy: 2. Determination of the “power” of therapeutic trials based on the natural history. *Muscle Nerve* 6, 91–103.
- Cardone, N., Taglietti, V., Baratto, S., Kefi, K., Periou, B., Gitiaux, C., Barnerias, C.,

- Lafuste, P., Pharm, F.L., Pharm, J.N., Panicucci, C., Desguerre, I., Bruno, C., Authier, F.-J., Fiorillo, C., Relaix, F., Malfatti, E., 2023. Myopathologic trajectory in Duchenne muscular dystrophy (DMD) reveals lack of regeneration due to senescence in satellite cells. *Acta Neuropathol Commun* 11, 167.
- Cheng, D.O., Khaw, C.R., McCabe, J., Pennycuick, A., Nair, A., Moore, D.A., Janes, S.M., Jacob, J., 2024. Predicting histopathological features of aggressiveness in lung cancer using CT radiomics: a systematic review. *Clin Radiol* 79, 681–689.
- Crisafulli, S., Sultana, J., Fontana, A., Salvo, F., Messina, S., Trifirò, G., 2020. Global epidemiology of Duchenne muscular dystrophy: an updated systematic review and meta-analysis. *Orphanet J Rare Dis* 15, 141.
- Dang, U.J., Damsker, J.M., Guglieri, M., Clemens, P.R., Perlman, S.J., Smith, E.C., Horrocks, I., Finkel, R.S., Mah, J.K., Deconinck, N., Goemans, N.M., Haberlová, J., Straub, V., Mengle-Gaw, L., Schwartz, B.D., Harper, A., Shieh, P.B., De Waele, L., Castro, D., Yang, M.L., Ryan, M.M., McDonald, C.M., Tulinius, M., Webster, R.I., Mcmillan, H.J., Kuntz, N., Rao, V.K., Baranello, G., Spinty, S., Childs, A.-M., Sbrocchi, A.M., Selby, K.A., Monduy, M., Nevo, Y., Vilchez, J.J., Nascimento-Osorio, A., Niks, E.H., De Groot, I.J.M., Katsalouli, M., Van Den Anker, J.N., Ward, L.M., Leinonen, M., D'Alessandro, A.L., Hoffman, E.P., 2024. Efficacy and Safety of Vamorolone Over 48 Weeks in Boys With Duchenne Muscular Dystrophy: A Randomized Controlled Trial. *Neurology* 102, e208112.
- Desguerre, I., Mayer, M., Leturcq, F., Barbet, J.-P., Gherardi, R.K., Christov, C., 2009. Endomysial fibrosis in Duchenne muscular dystrophy: a marker of poor outcome associated with macrophage alternative activation. *J Neuropathol Exp Neurol* 68, 762–73.
- Ding, X., Li, Z., Lin, G., Li, W., Xue, L., 2022. Toll-7 promotes tumour growth and invasion in Drosophila. *Cell Prolif* 55, e13188.
- Duan, D., 2018. Systemic AAV Micro-dystrophin Gene Therapy for Duchenne Muscular Dystrophy. *Mol Ther* 26, 2337–2356.
- Duan, D., Goemans, N., Takeda, S., Mercuri, E., Artsma-Rus, A., 2021. Duchenne muscular dystrophy. *Nat Rev Dis Primers* 7.
- Dubuisson, N., Versele, R., Planchon, C., Selvais, C.M., Noel, L., Abou-Samra, M., Davis-López de Carrizosa, M.A., 2022. Histological Methods to Assess Skeletal Muscle Degeneration and Regeneration in Duchenne Muscular Dystrophy. *Int J Mol Sci* 23.
- Egan, K.P., Brennan, T.A., Pignolo, R.J., 2012. Bone histomorphometry using free and

- commonly available software. *Histopathology* 61, 1168–73.
- Elangkovan, N., Dickson, G., 2021. Gene Therapy for Duchenne Muscular Dystrophy. *J Neuromuscul Dis* 8, S303–S316.
- Erkut, E., Yokota, T., 2022. CRISPR Therapeutics for Duchenne Muscular Dystrophy. *Int J Mol Sci* 23.
- Fang, Y., McDonald, C.M., Clemens, P.R., Gordish, H.-D., Illei, K., Hoffman, E.P., CINRG DNHS and Vamorolone 002/003/LTE Investigators, Dang, U.J., 2023. Modeling Early Heterogeneous Rates of Progression in Boys with Duchenne Muscular Dystrophy. *J Neuromuscul Dis* 10, 349–364.
- Finanger, E.L., Russman, B., Forbes, S.C., Rooney, W.D., Walter, G.A., Vandenborne, K., 2012. Use of skeletal muscle MRI in diagnosis and monitoring disease progression in Duchenne muscular dystrophy. *Phys Med Rehabil Clin N Am* 23, 1–10, ix.
- Fitzgerald, S., Wang, S., Dai, D., Murphree, D.H., Pandit, A., Douglas, A., Rizvi, A., Kadirvel, R., Gilvarry, M., McCarthy, R., Stritt, M., Gounis, M.J., Brinjikji, W., Kallmes, D.F., Doyle, K.M., 2019. Orbit image analysis machine learning software can be used for the histological quantification of acute ischemic stroke blood clots. *PLoS One* 14, e0225841.
- Fontaine Carbonnel, S., Dabaj, I., de Montferrand, C., Rippert, P., Laugel, V., De Lucia, S., Ravelli, C., Seferian, A., Ropars, J., Cancès, C., 2024. Choice of compound, dosage, and management of side effects for long-term corticosteroid treatment in Duchenne muscular dystrophy: Guidelines from the Neuromuscular Commission of the French Society of Pediatric Neurology. *Arch Pediatr* 31, 410–418.
- Frank, D.E., Schnell, F.J., Akana, C., El-Husayni, S.H., Desjardins, C.A., Morgan, J., Charleston, J.S., Sardone, V., Domingos, J., Dickson, G., Straub, V., Guglieri, M., Mercuri, E., Servais, L., Muntoni, F., SKIP-NMD Study Group, 2020. Increased dystrophin production with golodirsen in patients with Duchenne muscular dystrophy. *Neurology* 94, e2270–e2282.
- Gelman, A., Carlin, J., Stern, H., Dunson, D., Vehtari, A., Rubin, D., 2025. Bayesian Data Analysis Third edition (electronic edition) [WWW Document]. URL <https://sites.stat.columbia.edu/gelman/book/BDA3.pdf> (accessed 5.6.25).
- Guglieri, M., Clemens, P.R., Perlman, S.J., Smith, E.C., Horrocks, I., Finkel, R.S., Mah, J.K., Deconinck, N., Goemans, N., Haberlova, J., Straub, V., Mengle-Gaw, L.J., Schwartz, B.D., Harper, A.D., Shieh, P.B., De Waele, L., Castro, D., Yang, M.L., Ryan, M.M., McDonald, C.M., Tulinius, M., Webster, R., McMillan, H.J., Kuntz,

- N.L., Rao, V.K., Baranello, G., Spinty, S., Childs, A.-M., Sbrocchi, A.M., Selby, K.A., Monduy, M., Nevo, Y., Vilchez-Padilla, J.J., Nascimento-Osorio, A., Niks, E.H., de Groot, I.J.M., Katsalouli, M., James, M.K., van den Anker, J., Damsker, J.M., Ahmet, A., Ward, L.M., Jaros, M., Shale, P., Dang, U.J., Hoffman, E.P., 2022. Efficacy and Safety of Vamorolone vs Placebo and Prednisone Among Boys With Duchenne Muscular Dystrophy: A Randomized Clinical Trial. *JAMA Neurol* 79, 1005–1014.
- Happi Mbakam, C., Lamothe, G., Tremblay, G., Tremblay, J.P., 2022. CRISPR-Cas9 Gene Therapy for Duchenne Muscular Dystrophy. *Neurotherapeutics* 19, 931–941.
- Hollingsworth, K.G., Garrood, P., Eagle, M., Bushby, K., Straub, V., 2013. Magnetic resonance imaging in Duchenne muscular dystrophy: longitudinal assessment of natural history over 18 months. *Muscle Nerve* 48, 586–8.
- James, G., Witten, D., Hastie, T., Tibshirani, R., 2021. An Introduction to Statistical Learning. Springer US, New York, NY.
- Jiang, C., Luo, Y., Yuan, J., You, S., Chen, Z., Wu, M., Wang, G., Gong, J., 2020. CT-based radiomics and machine learning to predict spread through air space in lung adenocarcinoma. *Eur Radiol* 30, 4050–4057.
- Jütte, L., Yang, Z., Sharma, G., Roth, B., 2022. Focus stacking in non-contact dermoscopy. *Biomed Phys Eng Express* 8.
- Kass, R.E., Raftery, A.E., 1995. Bayes Factors. *J Am Stat Assoc* 90, 773–795.
- Kass, R.E., Wasserman, L., 1995. A Reference Bayesian Test for Nested Hypotheses and its Relationship to the Schwarz Criterion. *J Am Stat Assoc* 90, 928–934.
- Lakens, D., 2022. Improving Your Statistical Inferences [WWW Document]. Online Publish. URL https://lakens.github.io/statistical_inferences/ (accessed 4.27.25).
- Li, D.D.-U., Arlt, J., Tyndall, D., Walker, R., Richardson, J., Stoppa, D., Charbon, E., Henderson, R.K., 2011. Video-rate fluorescence lifetime imaging camera with CMOS single-photon avalanche diode arrays and high-speed imaging algorithm. *J Biomed Opt* 16, 096012.
- Mathur, S., Lott, D.J., Senesac, C., Germain, S.A., Vohra, R.S., Sweeney, H.L., Walter, G.A., Vandenborne, K., 2010. Age-related differences in lower-limb muscle cross-sectional area and torque production in boys with Duchenne muscular dystrophy. *Arch Phys Med Rehabil* 91, 1051–8.
- Matthews, E., Brassington, R., Kuntzer, T., Jichi, F., Manzur, A.Y., 2016. Corticosteroids for the treatment of Duchenne muscular dystrophy. *Cochrane Database Syst Rev* 2016, CD003725.

- Mayhew, A.G., Moat, D., McDermott, M.P., Eagle, M., Griggs, R.C., King, W.M., James, M.K., Muni-Lofra, R., Shillington, A., Gregson, S., Pallant, L., Skura, C., Staudt, L.A., Eichinger, K., McMurchie, H., Rabb, R., Di Marco, M., Brown, S., Zanin, R., Arnoldi, M.T., McIntyre, M., Wilson, A., Alfano, L.N., Lowes, L.P., Blomgren, C., Milev, E., Iodice, M., Pasternak, A., Chiu, A., Lehnert, I., Claus, N., Dieruf, K.A., Rolle, E., Nicorici, A., Andres, B., Hobbiebrunken, E., Roetmann, G., Kern, V., Civitello, M., Vogt, S., Hayes, M.J., Scholtes, C., Lacroix, C., Gunn, T., Warner, S., Newman, J., Barp, A., Kundrat, K., Kovelman, S., Powers, P.J., Guglieri, M., Muscle Study Group and TREAT-NMD, 2022. Functional outcome measures in young, steroid-naïve boys with Duchenne muscular dystrophy. *Neuromuscul Disord* 32, 460–467.
- Mcdonald, C.M., Henricson, E.K., Abresch, R.T., Florence, J.M., Eagle, M., Gappmaier, E., Glanzman, A.M., Spiegel, R., Barth, J., Elfring, G., Reha, A., Peltz, S., 2013. THE 6-minute walk test and other endpoints in Duchenne muscular dystrophy: Longitudinal natural history observations over 48 weeks from a multicenter study. *Muscle Nerve* 48, 343–356.
- Mendell, J.R., Rodino-Klapac, L.R., Sahenk, Z., Roush, K., Bird, L., Lowes, L.P., Alfano, L., Gomez, A.M., Lewis, S., Kota, J., Malik, V., Shontz, K., Walker, C.M., Flanigan, K.M., Corridore, M., Kean, J.R., Allen, H.D., Shilling, C., Melia, K.R., Sazani, P., Saoud, J.B., Kaye, E.M., 2013. Eteplirsen for the treatment of Duchenne muscular dystrophy. *Ann Neurol* 74, 637–647.
- Mendell, J.R., Sahenk, Z., Lehman, K., Nease, C., Lowes, L.P., Miller, N.F., Iammarino, M.A., Alfano, L.N., Nicholl, A., Al-Zaidy, S., Lewis, S., Church, K., Shell, R., Cripe, L.H., Potter, R.A., Griffin, D.A., Pozsgai, E., Dugar, A., Hogan, M., Rodino-Klapac, L.R., 2020. Assessment of Systemic Delivery of rAAVrh74.MHCK7.micro-dystrophin in Children With Duchenne Muscular Dystrophy: A Nonrandomized Controlled Trial. *JAMA Neurol* 77, 1122–1131.
- Min, Y.-L., Bassel-Duby, R., Olson, E.N., 2019. CRISPR Correction of Duchenne Muscular Dystrophy. *Annu Rev Med* 70, 239–255.
- Moreno, S., Bonfante, M., Zurek, E., Cherezov, D., Goldgof, D., Hall, L., Schabath, M., 2021. A Radiogenomics Ensemble to Predict EGFR and KRAS Mutations in NSCLC. *Tomography* 7, 154–168.
- Muggeo, V.M.R., 2003. Estimating regression models with unknown break-points. *Stat Med* 22, 3055–71.
- Nakagawa, S., Cuthill, I.C., 2007. Effect size, confidence interval and statistical

- significance: a practical guide for biologists. *Biol Rev Camb Philos Soc* 82, 591–605.
- Nonaka, I., Nishino, I., 2021. Muscle Pathology for Clinical Practice, 5th ed. Nihon Iji Shinpo Sha, Tokyo.
- Peduzzi, P., Concato, J., Kemper, E., Holford, T.R., Feinstein, A.R., 1996. A simulation study of the number of events per variable in logistic regression analysis. *J Clin Epidemiol* 49, 1373–9.
- Peverelli, L., Testolin, S., Villa, L., D'Amico, A., Petrini, S., Favero, C., Magri, F., Morandi, L., Mora, M., Mongini, T., Bertini, E., Sciacco, M., Comi, G.P., Moggio, M., 2015. Histologic muscular history in steroid-treated and untreated patients with Duchenne dystrophy. *Neurology* 85, 1886–93.
- Pinheiro, G., Pereira, T., Dias, C., Freitas, C., Hespanhol, V., Costa, J.L., Cunha, A., Oliveira, H.P., 2020. Identifying relationships between imaging phenotypes and lung cancer-related mutation status: EGFR and KRAS. *Sci Rep* 10, 3625.
- Rinaldi, L., Guerini Rocco, E., Spitaleri, G., Raimondi, S., Attili, I., Ranghiero, A., Cammarata, G., Minotti, M., Lo Presti, G., De Piano, F., Bellerba, F., Funicelli, G., Volpe, S., Mora, S., Fodor, C., Rampinelli, C., Barberis, M., De Marinis, F., Jereczek-Fossa, B.A., Orecchia, R., Rizzo, S., Botta, F., 2023. Association between Contrast-Enhanced Computed Tomography Radiomic Features, Genomic Alterations and Prognosis in Advanced Lung Adenocarcinoma Patients. *Cancers (Basel)* 15, 4553.
- Rouder, J.N., Speckman, P.L., Sun, D., Morey, R.D., Iverson, G., 2009. Bayesian t tests for accepting and rejecting the null hypothesis. *Psychon Bull Rev* 16, 225–37.
- Sanderson, M.J., Smith, I., Parker, I., Bootman, M.D., 2014. Fluorescence microscopy. *Cold Spring Harb Protoc* 2014, pdb.top071795.
- Shiri, I., Amini, M., Nazari, M., Hajianfar, G., Haddadi Avval, A., Abdollahi, H., Oveisi, M., Arabi, H., Rahmim, A., Zaidi, H., 2022. Impact of feature harmonization on radiogenomics analysis: Prediction of EGFR and KRAS mutations from non-small cell lung cancer PET/CT images. *Comput Biol Med* 142, 105230.
- Shosekai-Kenkyujo, 2021. Kenbikyo Tettei Customize Guide [Complete Guide to Microscope Customization]. Shosekai-Kenkyujo, Tokyo.
- Sun, C., Serra, C., Lee, G., Wagner, K.R., 2020. Stem cell-based therapies for Duchenne muscular dystrophy. *Exp Neurol* 323, 113086.
- Takeda, S., Clemens, P.R., Hoffman, E.P., 2021. Exon-Skipping in Duchenne Muscular Dystrophy. *J Neuromuscul Dis* 8, S343–S358.

- van Dommelen, P., van Dijk, O., de Wilde, J.A., Verkerk, P.H., 2024. Short developmental milestone risk assessment tool to identify Duchenne muscular dystrophy in primary care. *Orphanet J Rare Dis* 19, 192.
- Volinsky, C.T., Raftery, A.E., 2000. Bayesian information criterion for censored survival models. *Biometrics* 56, 256–62.
- Walters, J., 2017. Muscle hypertrophy and pseudohypertrophy. *Pract Neurol* 17, 369–379.
- Yamakado, T., Sato-Yazawa, H., Ishii, J., Kashiwagi, K., Kimura, T., Tanei, Z.-I., Yazawa, T., Ishida, Y., Tanaka, S., 2025. Spontaneous Transformation from Lung Adenocarcinoma to MYC-amplified Large Cell Neuroendocrine Carcinoma. *Pathol Int* 75, 105–113.
- Yamakado, T., Tanei, Z., Ishikawa, Y., Kimura, T., Ishida, Y., Tanaka, S., 2024. Sporadic gastric foveolar-type adenoma with morular metaplasia. *Pathol Int* 74, 489–492.
- Zatz, M., Rapaport, D., Vainzof, M., Passos-Bueno, M.R., Bortolini, E.R., Pavanello, R. de C., Peres, C.A., 1991. Serum creatine-kinase (CK) and pyruvate-kinase (PK) activities in Duchenne (DMD) as compared with Becker (BMD) muscular dystrophy. *J Neurol Sci* 102, 190–6.
- Zhou, Y., Ru, G.Q., Yan, R., Wang, M.S., Chen, M.J., Yu, L.L., Wang, H., 2017. An Inexpensive Digital Image Analysis Technique for Liver Fibrosis Quantification in Chronic Hepatitis B Patients. *Ann Hepatol* 16, 881–887.